
Article:
DYKEMAN, ERIC CHARLES (2025) An empirical model of aminoacylation kinetics for E. coli class I and II aminoacyl tRNA synthetases. PLoS Computational Biology. e1013353. ISSN: 1553-7358

https://doi.org/10.1371/journal.pcbi.1013353

PLOS COMPUTATIONAL BIOLOGY

RESEARCH ARTICLE

An empirical model of aminoacylation kinetics for *E. coli* class I and II aminoacyl tRNA synthetases

Eric C. Dykeman*

Department of Mathematics, University of York, York, United Kingdom

* eric.dykeman@york.ac.uk

OPEN ACCESS

Citation: Dykeman EC (2025) An empirical model of aminoacylation kinetics for *E. coli* class I and II aminoacyl tRNA synthetases. PLoS Comput Biol 21(8): e1013353. https://doi.org/10.1371/journal.pcbi.1013353

Editor: Stacey D. Finley, University of Southern California, UNITED STATES OF AMERICA

Received: September 3, 2024

Accepted: July 21, 2025

Published: August 12, 2025

Data availability statement: Software used in the simulations can be downloaded from https://www-users.york.ac.uk/~ecd502/ or from Github at https://github.com/edykeman/ribosome-aars.

Funding: The author(s) received no specific funding for this work.

Competing interests: The authors have declared that no competing interests exist.

Abstract

Efficient functioning of the prokaryotic translational system depends on a steady supply of aminoacylated tRNAs to be delivered to translating ribosomes via ternary complex. As such, tRNA synthetases play a crucial role in maintaining efficient and accurate translation in the cell, as they are responsible for aminoacylating the correct amino acid to its corresponding tRNA. Moreover, the kinetic rate at which they perform this reaction will dictate the overall rate of supply of aminoacylated tRNAs to the ribosome and will have consequences for the average translational speed of ribosomes in the cell. In this work, I develop an empirical kinetic model for the 20 aminoacyl tRNA synthetase enzymes in *E. coli* enabling the study of the effects of tRNA charging dynamics on translational efficiency. The model is parametrised based on *in vitro* experimental measurements of substrate K_m and k_{cat} values for both pyrophosphate exchange and aminoacylation. The model also reproduces the burst kinetics observed in class I enzymes and the transfer rates measured in single turnover experiments. Stochastic simulation of *in vivo* translation shows the kinetic model is able to support the tRNA charging demand resulting from translation in exponentially growing *E. coli* cells at a variety of different doubling times. This work provides a basis for the theoretical study of the amino acid starvation and the stringent response, as well as the complex behaviour of tRNA charging and translational dynamics in response to cellular stresses.

Author summary

Elucidating the complex interplay between tRNA charging by aminoacyl tRNA synthetases and the overall ribosomal demand for tRNAs will have important consequences for understanding the effects of amino acid starvation and the stringent response. Here I introduce an empirical kinetic model of the 20 *E. coli* tRNA synthetases and examine tRNA charging dynamics during exponential growth. The results show that the model is in good agreement with a variety of experimental observations, such as tRNA charging

fractions, average translational speed of the ribosome, and measured total cellular tRNA abundances.

Introduction

Understanding the functioning of the translational machinery in bacteria has the potential to impact a wide variety of fields in microbiology, such as understanding the effects of antibiotics which target ribosomes or aminoacyl tRNA synthetases, or in the development of efficient cell free protein synthesis systems. A key aspect of the protein translational apparatus of all cells is the aminoacylation of tRNAs, where amino acids are covalently linked to tRNAs for subsequent delivery to translating ribosomes. This action, sometimes referred to as tRNA charging, is performed via one of the 20 aminoacyl tRNA synthetases which are responsible for ensuring accuracy in the translation of the genetic code by covalently linking the correct amino acid to the correct tRNA. However, in order to theoretically and computationally study how tRNA synthetases affect the translational process, the creation of a model of tRNA charging by tRNA synthetases is required.

Since roughly the mid 1960's, there has been tremendous work on elucidating the kinetic mechanism of tRNA charging by aminoacyl tRNA synthetases (AARS). Pioneering experimental work on AARSs started with the examination of their pyrophosphate exchange kinetics [1]. Using radio labelled pyrophosphate, researchers monitored the conversion of radioactive pyrophosphate into radioactive ATP by AARSs which could be isolated using thin-layer chromatography. Later work began to look at both pyrophosphate exchange kinetics and the overall aminoacylation reaction by radio labelling the amino acid and monitoring the production of radioactive aa-tRNAs [2]. These experiments started to provide data on the kinetic behaviour of different AARSs, specifically the k_{cat} and K_m values of the three different substrates (amino acid, ATP, and tRNA) along with details of the overall steady-state kinetics. Subsequent kinetic experiments examined the behaviour of several AARSs under single-turnover conditions (i.e. where enzyme is in excess over tRNA), allowing estimations of the kinetic rates of amino acid transfer to the tRNA (k_{tran}) and of the overall chemistry step (k_{chem}), which is a composite rate that includes the formation of amino acid adenylate complex along with the transfer step and formation of aminoacylated tRNA [3].

This work, together with structural data of AARSs in complex with various substrates, has allowed a fairly descriptive picture to emerge of the kinetic steps which take place on these enzymes and a classification into two main classes based on their observed kinetic properties [4,5]. Class I AARSs are mostly monomeric and usually display burst kinetics of aminoacyl tRNA (aa-tRNA) formation, while Class II AARSs are dimers and display no burst kinetics. Here burst kinetics describes a property of the enzyme in which there is an initial burst of aa-tRNA production at a rate greater then the k_{cat} of the enzyme followed by the steady state aa-tRNA production rate. Table A in S1 Text summarises the classes for each of the AARS enzymes in *E. Coli*.

While experimental measurements of AARS enzymes have had sufficient time to develop over the last 50-60 years, there has been limited attempts to computationally model, or reproduce empirically, the experimental observations of AARS kinetics. Airas [6,7] used experimental observations of tRNA charging kinetics for class I argRS and ileRS to estimate a set of best fit kinetic parameters for a theoretical model. However, it is unclear if these models reproduce burst kinetics for these enzymes. On the other hand, Santra and Bagchi [8] provide ODE models of tRNA charging kinetics for both class I and class II AARS enzymes where their kinetic models are able to demonstrate burst and non-burst kinetics. In this work, the

authors consider product release as the rate limiting step in a model of Class I cysRS kinetics, which reproduced the burst kinetics reported in Zhang et al. [9]. For class II enzymes, they introduce an amino acid activation pathway in the presence of tRNA which was much slower than the activation in the absence of tRNA [8]. This resulted in steady state kinetics that displayed no pre-steady state burst. However, despite the success of their model in reproducing burst kinetics, it is unclear if their models would accurately reproduce experimentally observed K_m measurements for the substrates.

More recently, Choi and Covert have attempted to develop a Michaelis–Menten model for all 20 *E. coli* aminoacyl tRNA synthetases [10]. Their model is developed based on a review of the experimental literature of *in vitro* k_{cat} and K_m measurements, which have been subsequently optimised to support the translation speed required to double the *E. coli* proteome in a model of the *E. coli* cell cycle [11]. While such a model should potentially reproduce experimentally observed K_m measurements for the substrates, it ignores subtle features of the AARS enzymes such as burst kinetics.

The goal of this work is to develop an empirical kinetic model, similar to the models of Airas and/or Santra and Bagchi, which details the individual kinetic steps of aminoacylation reaction whilst also reproducing burst kinetics and experimentally observed K_m measurements for the substrates. The development of an empirical model of AARS kinetics can be useful for several reasons. First, in a bacterial cell such as *E. coli*, several important questions remain regarding tRNA charging and turnover by AARSs during ribosome elongation on messenger RNA (mRNA). One such question relates to the effect on tRNA charging during amino acid starvation and the activation of the stringent response. Work by Elf et al. examined a simple model of tRNA charging competition between different tRNA isoacceptors after amino acid starvation [12,13]. However, a more detailed model that also accounts for K_m values of amino acid can also look at, for example, regimes just at the threshold of starvation, where there may also be subtle effects on the charging levels of tRNAs [13].

The paper is outlined as follows. First, I create an empirical kinetic model for all 20 aminoacyl tRNA synthetases of *E. coli* which recapitulate their observed kinetic properties *in vitro*. Here, the observed kinetic properties are their k_{cat}, K_m, and single turnover rates k_{tran} and k_{chem}. Second, using these models combined with proteomics data for *E. coli* growing under controlled chemostat conditions in the exponential phase, I demonstrate that the observed *in vitro* kinetic rates (k_{cat} and K_m) are roughly in line with the k_{cat} values that would be required to supply charged tRNAs to elongating ribosomes *in vivo*, with a few enzymes requiring a small adjustment (by a factor of 2 on average) to their k_{cat}. This is in contrast to the recent model of Choi and Covert [10] where the Authors report that the majority of enzymes require, on average, a 7-fold increase in their k_{cat} values to support observed *in vivo* charging rates. Finally, I discuss some of the issues in creating a Michaelis–Menten model of tRNA synthetases, and compare my results with the recent model reported by Choi and Covert [10].

Methods

Aminoacyl tRNA synthetase kinetic model construction

Development of an empirical model of AARS kinetics requires two main steps; first a description of the individual kinetic steps involved in the charging of tRNAs with amino acids, and second, a method for fitting the kinetic rates such that the experimentally observed kinetic properties of the enzyme are reproduced by the model. Amino acid charging of tRNAs by aminoacyl tRNA synthetases occurs via a two step mechanism consisting of amino acid activation (Eq 1) and amino acid transfer (Eq 2), as described below. It is critically important to

note that both of these steps are catalytic events and hence each have their own k_{cat} and K_m values for the reactions. In the first step, amino acid and ATP bind to the enzyme, forming an amino acid adenylate (AMP-aa), followed by release of pyrophosphate (activation) [4,5]. The amino acid adenylate reaction can occur with or without tRNA present on the enzyme, except in the three class I enzymes argRS, gluRS and glnRS, which specifically require tRNA to be present for activation to occur [4]. In the second step, the amino acid is transferred from the adenylate to the tRNA to form the charged aa-tRNA (transfer) [4,5]. While the basic reaction scheme of the two-step process is described by Eqs. 1 and 2, this does not form a complete kinetic picture of the individual reactions (binding of ATP, dissociation of pyrophosphate etc.) which occur, nor the kinetic order of these events.

$$\mathrm{E} + \mathrm{ATP} + \mathrm{aa} \rightarrow \mathrm{E} \cdot \mathrm{AMP} - \mathrm{aa} + \mathrm{PPi} \quad (1)$$

$$\mathrm{E} \cdot \mathrm{AMP} - \mathrm{aa} + \mathrm{tRNA} \rightarrow \mathrm{E} + \mathrm{aa} - \mathrm{tRNA} + \mathrm{AMP} \quad (2)$$

In the next sections I give details on the individual kinetic steps that I consider in my model for both monomeric class I, dimeric class I, and dimeric class II AARS enzymes. In addition, I discuss the mathematical procedures used to calculate observed kinetic properties of the enzyme, (*i.e.* k_{cat}, K_m, k_{chem}, k_{tran}), and describe the general steps used to identify kinetic parameters for the model. Additional discussion of more technical information regarding the search of the multi-dimensional kinetic parameter space can be found in S1 Text.

Kinetic reaction scheme for monomeric class I tRNA synthetases. For the monomeric class I aminoacyl tRNA synthetases (cysRS, argRS, valRS, ileRS, leuRS, glnRS, and gluRS), I use the reaction scheme depicted in Fig 1a to model the full aminoacylation reaction. I also model the class I dimers tyrRS and trpRS using this scheme since tyrRS was shown to have half of sites activity [14,15] while trpRS was shown to bind tRNA asymmetrically across the dimer interface [16]. This asymmetric binding of tRNA in tyrRS implies that only one site of the dimer can be active at a time and thus essentially functions as a monomeric unit. The labelled states S_i with $i \in [0, 15]$ represent different states of the AARS enzyme, with S_0 representing the AARS enzyme free of all substrates. Specific details on each state of the enzyme, along with the labelled kinetic rates, are given by Fig C in S1 Text. All of the labelled kinetic rates in the diagram have both a forward and a backward rate (e.g. k_{2f} and k_{2b}), and I label dissociation constants for substrate binding reactions as $K_{2d} = k_{2b}/k_{2f}$. Only the general kinetic binding and chemical reaction steps are considered, and any conformational changes of the enzyme itself are ignored in the kinetic reaction scheme. Any editing reactions where the enzyme checks for mis-charged tRNAs are also not considered in this kinetic model.

While the reaction scheme may seem overly complicated, the following examples illustrate why all of these steps are required in order for the model to reproduce K_m values across both pyrophosphate exchange and aminoacylation experiments. Previous work on a detailed experimental analysis of isoleucine tRNA synthetase kinetics from *S. aureus* by Pope and colleagues [18] has shown that in the presence of tRNA, amino acid, and ATP, all three substrates bind to the enzyme in a random order before undergoing adenylate formation and aa-tRNA formation. As such, I have allowed the random binding of these substrates to occur and have also allowed adenylate to form with or without tRNA present (except for argRS, gluRS, and glnRS). If the kinetic steps of the model are simplified to consider an ordered binding of tRNA, amino acid, and ATP to the enzyme, then the predicted K_m for tRNA in the aminoacylation reaction is often drastically lower (usually by a factor of 10 or more) than what is measured experimentally. However, if a random binding of the three substrates is considered, as shown in

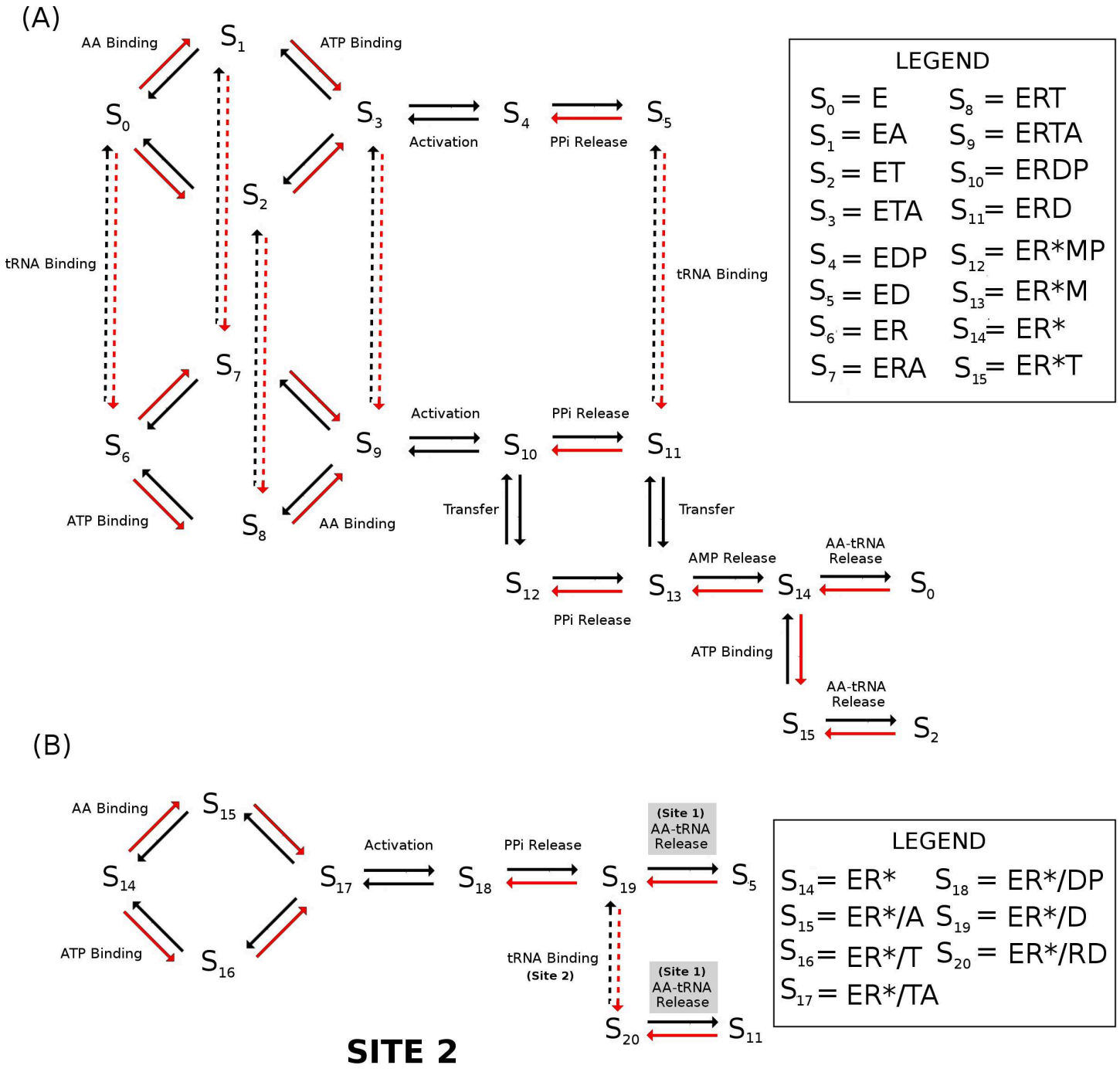

Fig 1. Kinetic reaction scheme for class I and class II tRNA synthetases. (A) Detailed map of the reaction pathway for monomeric class I AARS enzymes. The states of the enzyme S_i are given in the legend on the right with abbreviations E = AARS enzyme, T = ATP, M = AMP, P = PP_i, D = AA Adenylate, R = tRNA, and R* = AA-tRNA denoting the charged tRNA. For example, state S_0 corresponds to the enzyme free of all substrates while S_5 corresponds to the enzyme with bound amino acid adenylate. The two main catalytic events, activation of the amino acid to form amino acid adenylate plus pyrophosphate (activation), and transfer of the amino acid from the adenylate to the tRNA (transfer) are labelled. Red arrows denote reaction steps where a substrate associates to the enzyme. (B) The reaction pathway for class I dimer metRS and class II AARS enzymes follows the kinetic flip-flop mechanism reported in Guth et al. [17]. Here, the same kinetic steps in site 1 of the dimer occur as in the class I enzymes followed by a subsequent activation event in site 2 while charged aa-tRNA in site 1 remains bound. After activation in site 2, aa-tRNA is released from site 1. States with substrate bound in the first and second site are separated by a slash, *e.g.* state S_{15} with charged tRNA in the first site and AA is bound to the second catalytic site is denoted as ER*/A.

https://doi.org/10.1371/journal.pcbi.1013353.g001

Fig 1A, then the predicted K_m for tRNA can be easily parameterised to be within the range of K_m values measured experimentally, demonstrating the importance of having the full reaction scheme shown in Fig 1. Additionally, when tRNA is bound to the enzyme, I have also allowed for pyrophosphate release to occur either before or after transfer of the amino acid to the tRNA (path $S_{10} \rightarrow S_{11} \rightarrow S_{13}$ vs. path $S_{10} \rightarrow S_{12} \rightarrow S_{13}$). Without this dual pathway, K_ms for ATP and amino acid in the aminoacylation reaction are often drastically lower than what is measured experimentally. This same problem was also noticed by Pope and colleagues when constructing a kinetic model of ileRS from *S. aureus* [18] which caused them to propose a similar mechanism of amino acid transfer prior to pyrophosphate release. Moreover, several other experimentalists have postulated that pyrophosphate may stay bound during the amino acid transfer step in some AARSs [19]. Finally, the reaction path $S_{14} \rightarrow S_{15} \rightarrow S_0$ in which ATP binds to the enzyme prior to the release of the aa-tRNA product ensures that the AARS enzyme is not kinetically inhibited in the presence of cellular concentrations of AMP (estimated 125-250 μ M [20]) and/or pyrophosphate (estimated 250-500 μ M [21,22]). As ATP is at a higher concentration than AMP in the cell (9 mM [20]), this path allows for ATP binding to compete with AMP and drive release of charged tRNA.

Kinetic reaction scheme for dimeric class II tRNA synthetases. For the dimeric class II AARS enzymes (serRS, thrRS, proRS, hisRS, aspRS, asnRS, lysRS, alaRS, glyRS and pheRS), as well as the dimeric class I metRS, I use the reaction scheme depicted in Fig 1A and 1B to model the aminoacylation reaction. Here, I assume that the dimeric enzymes follow the flip-flop kinetic model as described in Guth et al. [17] for hisRS. The flip-flop kinetic model assumes amino acid adenylate is formed and transferred to a tRNA at site 1 of the enzyme following the kinetic steps of a class I enzyme (Fig 1A). Afterwards, the charged tRNA remains bound to site 1 while an additional amino acid adenylate is formed at site 2 as shown in Fig 1B. Subsequently, the charged tRNA is released from site 1 while an uncharged tRNA is recruited to site 2. I allow the charged tRNA at site 1 to be released after activation of the amino acid at site 2, regardless of whether tRNA is bound at site 2.

Identification of kinetic parameters for the model. For the reaction scheme of class I AARS in Fig 1A, there are 48 kinetic parameters that must be chosen, with the goal that the resulting kinetics predicted by the model (specifically the K_m and k_{cat} for the enzymes substrates) match experimental observations. At first, the prospect of identifying a set of 48 parameters which will reproduce experimental values of K_m and k_{cat} seems impossible, even with experimental input. However, the complexity of fitting the parameters can be drastically reduced if one performs the fitting in three separate stages and allows some parameters, such as the rate of formation of the adenylate in the presence or absence or tRNA, to be identical with each other. Moreover, tRNA, amino acid, and ATP have usually had their dissociation constants (K_d) to AARS enzymes measured, which allows for further complexity reductions.

The specific idea that I propose to use to identify the kinetic parameters has two parts. The first is to exploit the fact that experimentalists perform three separate assays to elucidate the kinetic properties of AARSs; (1) the pyrophosphate exchange assay, (2) the single turnover kinetics assay, and (3) the aminoacylation assay. While the aminoacylation assay examines the entire process (and thus depends on all 48 kinetic parameters), the pyrophosphate exchange and single turnover kinetics only examine a subsection of the reaction scheme and thus only depend on a subset of the kinetic parameters. Fig 2A illustrates the kinetic scheme for the pyrophosphate exchange (12 kinetic parameters), while Fig 2B shows the scheme for the single turnover assay measuring the transfer rate k_{tran} (8 kinetic parameters). Thus, by fitting first the single turnover reaction, followed by the pyrophosphate exchange,

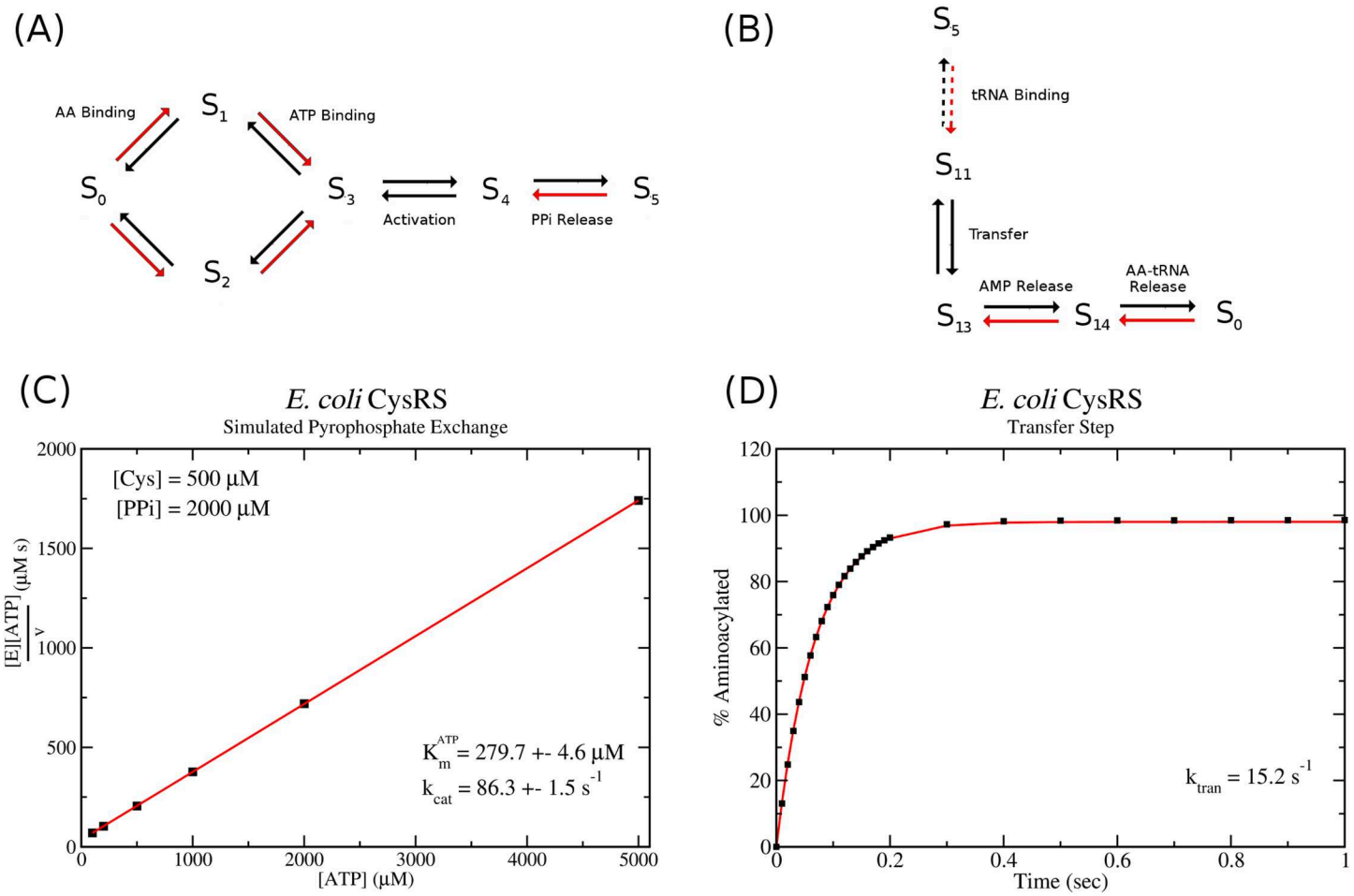

Fig 2. Computer simulation of pyrophosphate exchange and single turnover kinetics. (A) Reaction scheme used to simulate pyrophosphate exchange kinetics and, (B) reaction scheme used to simulate single turnover kinetics involving the transfer step. State notation follows that of Fig 1. (C) Example Woolf-Hanes plot and the resulting values of K_m^{atp} and k_{cat} from a computer simulation of pyrophosphate exchange for *E. coli* cysRS. (D) Example plot from a computer simulation of single turnover kinetics for *E. coli* cysRS. Black squares represent data points from the computer simulation while the red curve gives the best fit exponential $y(t) = A(1 - \exp(-k_{tran}t))$ to the data.

https://doi.org/10.1371/journal.pcbi.1013353.g002

one can slowly constrain parameters resulting in a smaller number to be varied in the final fitting of the aminoacylation assay. The second part relies on the observation that only a few of the kinetic parameters have an effect on the K_m or k_{cat} of the enzyme. For example, while the pyrophosphate exchange assay depends on 12 kinetic parameters, it can be shown through systematic variation of pairs of parameters that only 4 have a major effect on K_m or k_{cat} (see Fig B in S1 Text). While this implies that one can have a free choice for the other parameters, this is not how the fitting is done. Instead, the remaining parameters that have little or no effect on K_m or k_{cat} are chosen based on experimental measurements of dissociation constants (see S1 Spreadsheet which lists K_d measurements for each enzyme).

In many cases, the substrate parameters (either K_d or k_{on} and k_{off}) have been determined for a number of AARSs by *e.g.* fluorescence quenching [23] or pre-steady state kinetic measurements [24]. Kinetic parameters from these experimental measurements have been used in the models where available. For example, Bovee et al. [24] report a k_{on} and k_{off} for threonine

binding to thrRS:ATP of 0.024 $\mu M^{-1}s^{-1}$ and 3.2 s^{-1}, respectively. I found that direct use of these kinetic parameters results in a good correspondence between the model and experimental steady state values of K_m^{aa} for both pyrophosphate exchange and aminoacylation. Parameters with limited or no experimental data are varied following the algorithm in S1 Text until the kinetic properties of the enzyme predicted by the model (k_{cat}, K_m for each substrate, and k_{trans}, k_{chem}) match target values. These target values are typically the average of experimental data measurements, with outliers removed. The result is a set of parameters that reproduce the observed K_m and k_{cat} values for the enzyme, as well as any other kinetic behaviours, such as burst kinetics for the class I enzymes.

Calculation of k_{cat} and K_m in the kinetic model. As discussed above, there are three different experimental assays which examine different aspects of AARS kinetics. The first, pyrophosphate exchange, involves introducing radio labelled pyrophosphate to a mixture of ATP, amino acid, and enzyme with the reaction occurring according to the scheme shown in Fig 2A. ATP is then isolated by thin layer chromatography and its specific activity measured. Thus, this assay indirectly measures the rate of activation of the amino acid by measurement of the reverse process, *i.e.* the conversion of radioactive pyrophosphate and adenylate back to radioactive ATP and amino acid. The assay measures k_{cat} and K_m for both ATP and amino acid by fixing the concentration of one at saturating conditions then varying the concentration of the other. Cole and Schimmel [25] showed that the concentration of radioactive ATP (denoted ATP*) can be written as

$$\frac{d[ATP^*]}{dt} = V\frac{[PP^*]}{[PP]} - V\frac{[ATP^*]}{[ATP]}, \tag{3}$$

where V is the speed of the pyrophosphate exchange reaction. At $t = 0$ the amount of radioactive ATP is zero, and one obtains the relation for the initial speed of the conversion reaction as

$$\left.\frac{d[ATP^*]}{dt}\right|_{t=0} = V\left.\frac{[PP^*]}{[PP]}\right|_{t=0} = Vs(0), \tag{4}$$

where $s(t)$ is the specific activity of the pyrophosphate. Thus, one can directly simulate using either a stochastic or ODE based model the reaction scheme for pyrophosphate exchange using initial conditions matching experimental protocol. These initial conditions are usually $[PP]$ = 2 mM, $[ATP]$ = 5 mM, $[AA]$ = 0.5 – 1 mM, with initial enzyme concentration $[E]$ = 1 – 10 nM with a specific activity of $s = 0.02$. Varying either the initial ATP, PP, or amino acid concentrations while keeping the remaining substrates fixed, I simulate the pyrophosphate exchange scheme (Fig 2A) using the stochastic Gillespie algorithm. For each concentration of the varying substrate, the reaction kinetics are simulated 10 times, and the average and standard deviation of the initial reaction velocity V is computed. I then plot the velocity and concentration data using a Woolf-Hanes plot, which plots substrate concentration over the velocity versus substrate concentration. Linear regression is used to produce the best fit line ($y = mx + b$) and the slope of this line is $m = 1/k_{cat}$ while the line intercept is $b = K_m/k_{cat}$. Fig 2C shows an example of a K_m and k_{cat} calculation resulting from a computer simulation of pyrophosphate exchange for *E. coli* cysRS. The procedure is automated such that a parameter search can be employed by calling a function that returns k_{cat} and K_m and their standard error given initial substrate concentrations and a set of kinetic parameters. A near identical procedure can be done for the aminoacylation reaction schemes (Fig 1) where the production rate of aa-tRNA is monitored. Typical initial concentrations for the aminoacylation reactions are $[ATP]$ = 5 mM, $[AA]$ = 0.5 – 1 mM, $[tRNA]$ = 10 μM, and $[E]$ = 1 – 10 nM.

For the single turnover kinetics assay, the computer simulation and experiment measurements are slightly different. Here, the assay first pre-forms enzyme bound with adenylate (state S_5 in Figs 1 and 2B) and then isolates this enzyme complex. The adenylate contains a radio-labelled amino acid which will subsequently be transferred to a tRNA. The assay then proceeds with measuring this transfer rate under single turnover conditions, i.e. where concentration of the enzyme bound with radioactive adenylate is roughly 10x greater then the concentration of tRNA. Charged tRNAs are isolated at varying time points using thin-layer chromatography and the data are fit to the exponential function,

$$y(t) = A(1 - \exp(-Bt)), \tag{5}$$

with $B = k_{tran}$. In order to compare the model with this experiment, I simulate the tRNA charging reaction using the reaction scheme in Fig 2B and typical concentrations used in experiments ($[tRNA] = 5\ \mu$M, and $[E:Ad] = 50\ \mu$M). The formation of aa-tRNA as a function of time is output, and the results are fit to Eq 5. A similar single turnover assay which mixes ATP, amino acid, tRNA and enzyme simultaneously with enzyme 10x tRNA concentration can be used to measure the overall chemistry step k_{chem}. The inverse of k_{chem} approximates the average time required for the enzyme to bind all substrates, activate an amino acid, and transfer the amino acid to tRNA. Most single turnover assays observe that $k_{chem} \approx k_{tran}$ suggesting that binding of substrate and activation of the amino acid is fast compared with the final transfer step. Thus, k_{chem} can be used to confirm that the kinetic rates for substrate binding and amino acid activation in the model are sufficiently fast.

Computational simulations of *in vivo* translation and tRNA charging

Previously I developed a stochastic model of *in vivo* prokaryotic translation which takes into account protein synthesis on the full transcriptome present in an *E. coli* cell [26,27]. For example, in a typical *E. coli* cell which has a doubling time of $\tau = 60$ min, the model accounts for the protein synthesis occurring by roughly 15000 ribosomes on a transcriptome of roughly 2 million nucleotides of mRNA. In addition, the model also accounts for competition between mRNAs for available ribosomes as well as the competition for the A-site on the ribosome between different tRNA isoacceptors. Finally, since the translational model [26] takes into account each of the known individual kinetic steps in the translation process, the resulting elongation rate of the ribosomes emerges as a result of the codon bias in the mRNA and the concentration of tRNAs in ternary complex. Thus my model is capable of predicting the resulting change to the ribosome elongation rate that would result from any alteration to tRNA charging rates. The base code used in this work can be downloaded from Github at github.com/edykeman/ribofold and kinetic parameters used for the ribosome elongation steps can be found in [26]. Predictions of tRNA charging kinetics by AARS enzymes are incorporated into the stochastic ribosome model from [26] using the kinetic scheme in Fig 1. The individual kinetic parameters used in the model can be found in Tables B, C, and D in S1 Text. The translational model can also be run using a simplified Michaelis–Menten model for aminoacylation kinetics. Parameters used for the k_{cat} and K_m values are listed in Table I in S1 Text, with the optimized tRNA numbers for use with the Michaelis–Menten model given in Table J in S1 Text. Software used in the simulations can be downloaded from http://www-users.york.ac.uk/~ecd502/ or from Github at edykeman/ribosome-aars.

Construction of *E. coli* transcriptome

To construct the transcriptome for the stochastic model of translation, I have used mRNA-seq measurements from Li et al. [28] which give experimental measurements of the overall average numbers of individual mRNAs (in RPKM units) in the transcriptome. This information can be used to back construct a snapshot of the average transcriptome that would be observed in exponentially growing *E. coli* cells. To do this, I normalise the RPKM values ($n_R(i)$) for each mRNA type i, i.e.

$$x(i) = \frac{n_R(i)}{\sum_j n_R(j)}\,, \tag{6}$$

where the sum is over all mRNAs in the RNA-seq data. Then, I calculate the total number of mRNAs of each type via

$$n(i) = \alpha x(i)\,, \tag{7}$$

where α is a constant. The value α is chosen such that the total nucleotide content of the transcriptome approximately reproduces what has been estimated by Bremer and Dennis [29] for *E. coli* cells growing exponentially at growth rates of $\mu = 0.41, 0.69, 1.04$, and $1.73\ \mathrm{h}^{-1}$, *i.e.* doubling times $\tau = 100, 60, 40$, and 21 min. As a check, I calculate the codon bias in the predicted transcriptome and compare with the codon usage that was measured by a separate experiment reported in Dong et al. [30]. Tab C in S1 Spreadsheet shows that there is excellent agreement between the codon usage in the transcriptome versus what was measured in Dong et al.

Construction of violin plots

Consider a set of n measurements y_i with $i \in [1, n]$, each with an associated measurement error σ_i. Using this data set, I construct a violin plot $p(y)$ with $p(y) \in [0, 1]$ via

$$p(y) = \frac{1}{A}\sum_i^n \exp\left(-\frac{(y - y_i)^2}{2\sigma_i^2}\right), \tag{8}$$

where the constant A is chosen such that

$$\begin{aligned} A &= \sum_i^n \sqrt{2\pi}\sigma_i \\ 1 &= \int_{-\infty}^{\infty} p(y)\, dy\,. \end{aligned} \tag{9}$$

The function $p(y)$ can thus be considered as a probability density, where input of a particular value y gives an estimate of the probability that an experiment would measure this value. In the case of the proteomics data points, where no error value σ is usually given, I use a default 20% error value for the measurement.

Results

Empirical kinetic model of *E. coli* tRNA synthetases

I begin by discussing the kinetic models that have been constructed using the procedure in Methods for class I cysRS and class II hisRS enzymes from *E. Coli*. Cysteine tRNA synthetase is a monomeric class I enzyme which displays burst kinetics, while hisRS is a class II

enzyme which displays no burst kinetics in the pre-steady state. The kinetic properties of both enzymes (k_{cat}, K_m and k_{chem}, k_{tran} from single turnover assays) have been extensively measured *in vitro* by several different groups.

Table 1 gives the *in vitro* measurements of k_{cat} and K_m values for *E. coli* cysRS. Using this data, consensus K_m and k_{cat} values for the pyrophosphate exchange and aminoacylation assays can be estimated and, using the procedure outlined in Methods, a set of kinetic parameters which reasonably reproduce these values can be determined. Specifically for pyrophosphate exchange, the kinetic model gives values of $K_m^{aa} = 27\mu$M, $K_m^{atp} = 279\mu$M, and $k_{cat} = 85$ s^{-1}. Similarly for aminoacylation, the kinetic model gives values of $K_m^{aa} = 16\mu$M, $K_m^{trna} = 1.05\mu$M, and $k_{cat} = 2.96$ s^{-1}. Comparing with experiment, one can see that these values are within the range of those that have been measured experimentally (Fig 3A). Moreover, the identified parameters and kinetic model for cysRS reproduces the observed burst kinetics (Fig 3B) as well as the observed k_{tran} and k_{chem} values in simulations of single turnover kinetics (Fig 3C and 3D).

As with cysRS, Table 2 gives the *in vitro* measurements of k_{cat} and K_m values for *E. coli* hisRS. In this case, my fitting procedure (see Methods and S1 Text) has identified kinetic parameters for the kinetic model which, for pyrophosphate exchange, give values of $K_m^{aa} = 37\mu$M, $K_m^{atp} = 498\mu$M, and $k_{cat} = 130$ s^{-1}. Similarly for aminoacylation, the kinetic model gives values of $K_m^{aa} = 7.7\mu$M, $K_m^{trna} = 0.44\mu$M, and $k_{cat} = 7.2$ s^{-1}. As with cysRS, one can see that these values are within the range of those that have been measured experimentally for hisRS (Fig 4A). In addition, the identified parameters and kinetic model for hisRS results in no burst of charged his-tRNA^{his} (Fig 4B) as well as the observed k_{tran} and k_{chem} values in simulations of single turnover kinetics (Fig 4C and 4D).

As with cysRS and hisRS, I have also parametrised the remaining 18 tRNA synthetases from *E. coli* by identifying a set of kinetic parameters that reproduce experimental measurements for k_{cat} and K_m. Kinetic rates for each of the enzymes can be found in Tables B, C,

Table 1. In vitro measurements of *E. coli* cysRS K_m and k_{cat} values. The experimental measurements for three separate kinetic assays are reported for the Class I cysRS aminoacyl-tRNA synthetase enzyme. PMID denotes the PubMed ID for the reference source of the data. Abbreviations are, PP = pyrophosphate exchange, AA = aminoacylation, ST = single turnover transfer, and SC = single turnover overall chemistry. Units for k_{cat} are in s^{-1} and K_m are in μM.

PMID	Reaction	Substrate	kcat	Km	(kcat/Km)	Kch/Ktr	Temp	Date
12662918	PP	ATP	91 ± 40	290 ± 60	0.3138		37	2003
12974627	PP	ATP	142 ± 1.2	250 ± 2	0.5600		37	2003
30642164	PP	ATP	95 ± 4	271 ± 13	0.3506		37	2019
12662918	PP	CYS	79 ± 45	22 ± 11	3.5909		37	2003
12974627	PP	CYS	99.6 ± 7.8	31 ± 7	3.2129		37	2003
30642164	PP	CYS	88 ± 7	27 ± 3	3.2593		37	2019
14679218	AA	ATP	4.4 ± 0.34	338 ± 60	0.0130		30	2004
14679218	AA	CYS	4.8 ± 0.41	7.2 ± 1.0	0.6667		30	2004
16843487	AA	CYS	2.9 ± 0.1	22 ± 5	0.1318		37	2006
16843487	AA	tRNA	2.5 ± 0.06	1.2 ± 0.01	2.0833		37	2006
14679218	AA	tRNA	2.9 ± 0.17	0.64 ± 0.09	4.5313		30	2004
12662918	AA	tRNA	0.9 ± 0.03	0.35 ± 0.01	2.5714		37	2003
12974627	AA	tRNA	2.46 ± 0.06	1.16 ± 0.01	2.1207		37	2003
30642164	AA	tRNA	2.9 ± 0.4	1.4 ± 0.2	2.0714		37	2019
15489861	AA	tRNA	2.46 ± 0.06	1.16 ± 0.01	2.1207		37	2004
10860750	AA	tRNA	3.47 ± 0.12	1.54 ± 0.09	2.2532		37	2000
16843487	ST					14.9 ± 0.6	37	2006
16843487	SC					15.2 ± 0.5	37	2006

https://doi.org/10.1371/journal.pcbi.1013353.t001

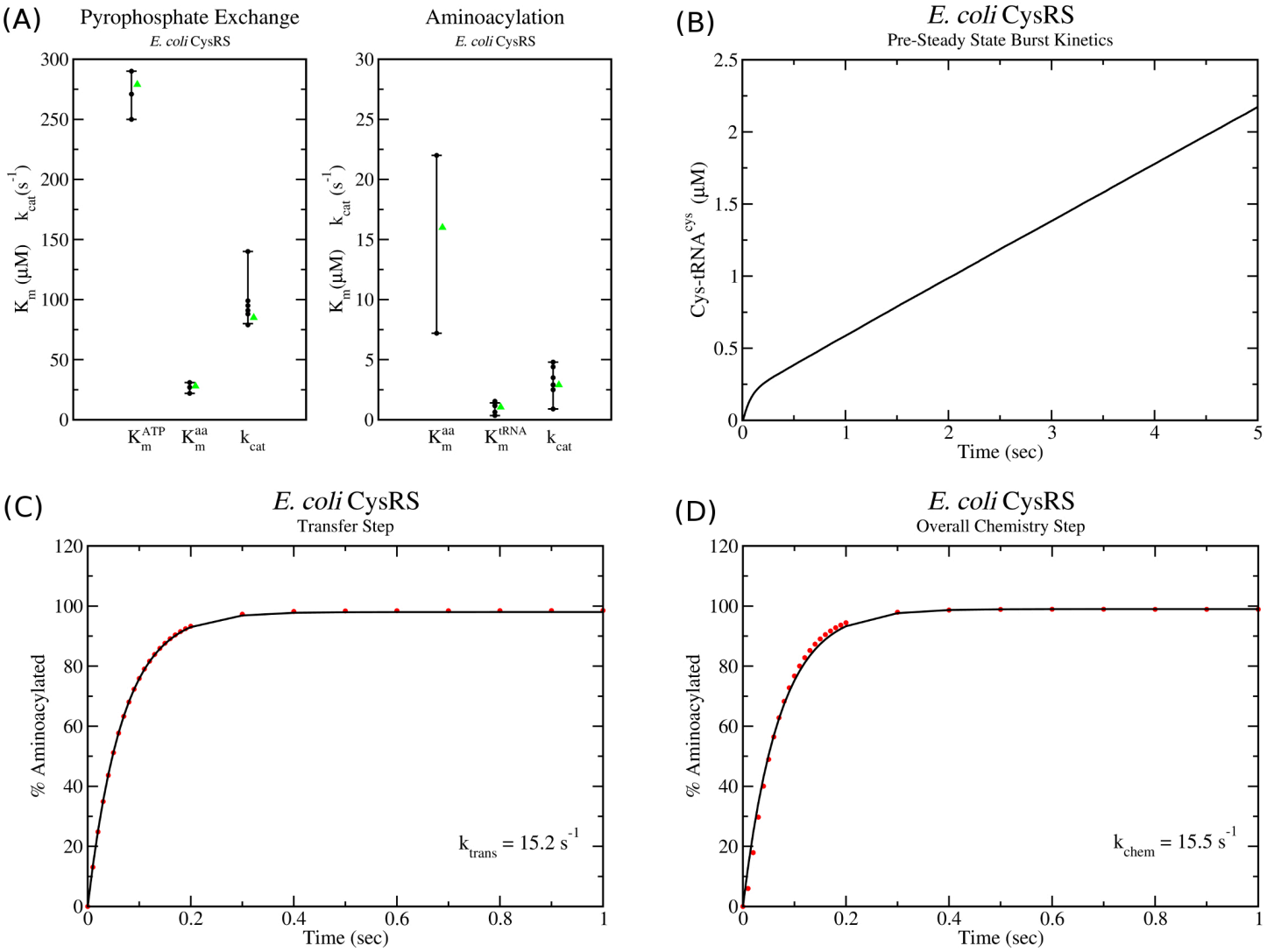

Fig 3. Kinetic model of class I cysRS tRNA charging. (A) Range of k_{cat} and K_m values determined by *in vitro* pyrophosphate and aminoacylation assays (black dots) are compared with the values of the kinetic model (green triangles). (B) Pre-steady state kinetics simulation with starting concentrations of $[cys] = 500\mu$M, $[ATP] = 5$ mM and $[tRNA] = 10\mu$M and $[E] = 0.25\mu$M show an initial burst of cys-tRNA charging followed by a slower steady state recapitulating what was observed experimentally in Ref. [9]. (C) Single turnover simulation of the transfer rate (k_{tran}) and (D) of the overall chemistry step (k_{chem}) show excellent agreement with experimentally observed values in Ref. [9].

https://doi.org/10.1371/journal.pcbi.1013353.g003

and D in S1 Text, while information on the experimental k_{cat} and K_m measurements and the models fit to them can be found in S1 Spreadsheet.

Optimization and validation of kinetic AARS models

Comparison of *in vivo* AARS activity with *in vitro* k_{cat} measurements. An important and critical question now arises regarding the k_{cat} and K_m values that have been measured experimentally *in vitro* for the aminoacyl tRNA synthetases. Specifically, are these *in vitro* measured k_{cat} and K_m values sufficient to support the tRNA charging rates observed *in vivo* in a typical exponentially growing *E. coli* cell. This question is complicated to answer for a number of reasons. First, bacterial cells undergoing exponential growth will have a cell cycle

Table 2. In vitro measurements of *E. coli* hisRS K_m and k_{cat} values. The experimental measurements for three separate kinetic assays are reported for the Class II hisRS aminoacyl-tRNA synthetase enzyme. PMID denotes the PubMed ID for the reference source of the data. Abbreviations are, PP = pyrophosphate exchange, AA = aminoacylation, ST = single turnover transfer, and SC = single turnover overall chemistry. Units for k_{cat} are in s^{-1} and K_m are in μM. nd/ns = not determined/stated.

PMID	Reaction	Substrate	kcat	Km	(kcat/Km)	Kch/Ktr	Temp	Date
9266856	PP	ATP	34 ± 3	560 ± 20	0.0607		37	1997
4591623	PP	ATP	nd	320	nd		ns	1974
30642164	PP	ATP	145 ± 37	763 ± 49	0.1900		37	2019
15751955	PP	ATP	130 ± 5	890 ± 64	0.1461		37	2005
11329259	PP	ATP	203 ± 5	675 ± 78	0.3007		37	2001
9131996	PP	ATP	120 ± 4	890 ± 64	0.1348		37	1997
4591623	PP	HIS	nd	100	nd		ns	1974
30642164	PP	HIS	120 ± 23	32 ± 4	3.7500		37	2019
15751955	PP	HIS	130 ± 5	30 ± 5	4.3333		37	2005
11329259	PP	HIS	133 ± 2	35.4 ± 4	3.7571		37	2001
9131996	PP	HIS	142 ± 5	30 ± 5	4.7333		37	1997
9266856	AA	HIS	7 ± 2	8 ± 2	0.8750		37	1997
4591623	AA	HIS	nd	6	nd		ns	1974
30642164	AA	tRNA	3.4 ± 0.5	0.7 ± 0.2	4.8571		37	2019
15751955	AA	tRNA	3.14	0.34	9.1176		37	2005
11329259	AA	tRNA	1.71 ± 0.06	0.34 ± 0.05	5.0294		37	2001
9131996	AA	tRNA	2.6 ± 0.4	1.4 ± 0.6	1.8571		37	1997
15751955	ST					18.8 ± 2.5	37	2005

https://doi.org/10.1371/journal.pcbi.1013353.t002

in which the number of proteins and ribosomes in the cell is increasing up until the point of cell division, after which the cellular contents are partitioned between the two daughter cells. Second, given a sample of cells growing at an average rate μ h^{-1} in a medium, the distribution of cells in the medium will be at different stages of the cell cycle, hence the cells will have different volumes as well as different numbers of ribosomes and proteins present. Finally, although the *average* growth rate of cells in the medium is μ, it is not clear that *all* cells in the medium will have this growth rate. Estimation of the average tRNA turnover by an AARS enzyme per cell is directly dependent on the growth rate (which determines tRNA/amino acid usage) and the number of AARS enzymes in the cell. Use of single cell proteomics measurements [31], which have been noted to contain a high amount of variation in protein numbers between cells, may present difficulties in determining the relation between the number of AARS proteins and the cellular growth rate.

Works by Bremer and Dennis as well as other colleagues in the field have shown that the macro-molecular composition of an *E. coli* cell growing exponentially in culture can be straightforwardly described by simple mathematical relations for the average cell in the medium [29]. Here I take a similar point of view and use, for instance, the amino acid usage rate that would occur *on average* in a exponentially growing culture of *E. coli* cells at an average growth rate of μ h^{-1}. Similarly, I calculate the average number of AARS enzymes that would be present and thus obtain the average tRNA turnover per enzyme. In order to determine the *in vivo* AARS activity from this point of view, one would require estimates of; (1) the average usage rate per second of each tRNA isoacceptor or alternatively the total rate of incorporation of each amino acid (a_i, $i \in [1, 20]$) into protein by ribosomes in the cell, (2) the average number of aminoacyl tRNA synthetases (n_i) in the cell, (3) the average number of tRNAs in the cell, and (4) the average volume of the cell. The amino acid usage and number of each AARS in the cell can be used to estimate the enzyme activity (r_i), *i.e.* the rate of tRNA

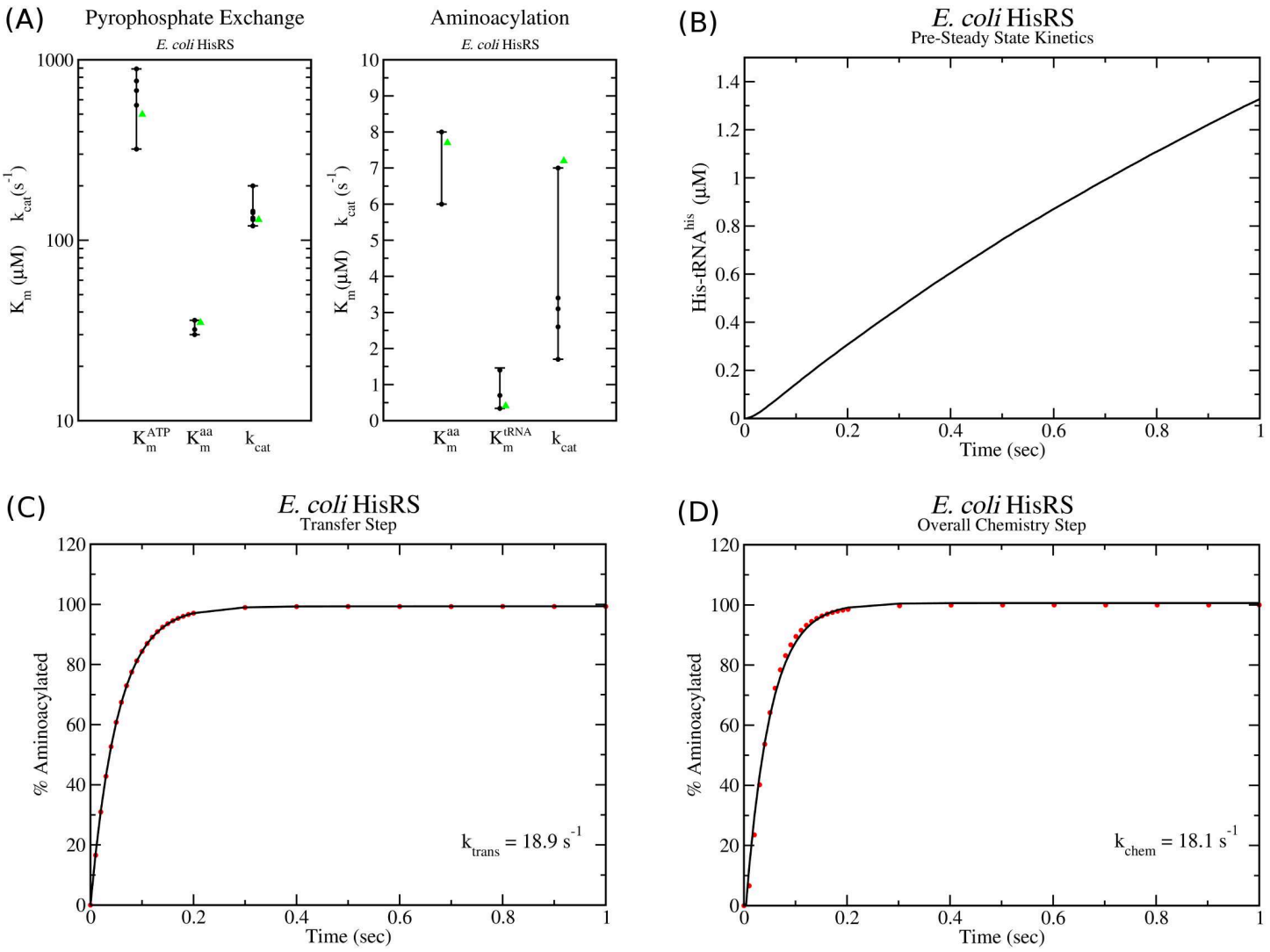

Fig 4. Kinetic model of class II hisRS tRNA charging. (A) Range of k_{cat} and K_m values determined by *in vitro* pyrophosphate and aminoacylation assays (black dots) are compared with the values of the kinetic model (green triangles). (B) Pre-steady state kinetics simulation with starting concentrations of $[his] = 500\mu$M, $[ATP] = 5$ mM and $[tRNA] = 10\mu$M and $[E] = 0.25\mu$M show no burst of his-tRNA charging as observed experimentally in [17]. (C) Single turnover simulation of the transfer rate (k_{tran}) and (D) of the overall chemistry step (k_{chem}) show excellent agreement with experimentally observed values in Ref. [17].

https://doi.org/10.1371/journal.pcbi.1013353.g004

turnover, for a single enzyme *in vivo*,

$$r_i = \frac{a_i}{n_i}. \tag{10}$$

The volume and number of tRNAs on the other hand can be used to determine if the resulting concentration of free uncharged tRNAs is sufficient to achieve a velocity (v_i) from the enzyme that is greater than or equal to the tRNA charging rate, $v_i \geq r_i$.

To estimate the number of each tRNA synthetase n_i, I have used 12 measurements of recent proteomics data across five different experimental groups [28,32–35]. These data points measure average protein abundances in exponentially growing *E. coli* across a variety of growth rates ($\mu = 0.41$ to $\mu = 1.98$ h^{-1}) where the elongation rates of ribosomes are estimated to vary between 12-22 aa/sec [29,36]. It is important to note that the amino acid and tRNA

isoacceptor usages are directly related to ribosome elongation rates, which are in turn dependent on the relative concentration of tRNA isoacceptors in ternary complex. Moreover, it has been observed that slower growing bacteria can undergo an immediate increase in protein synthesis following nutrient a up-shift [37] (see discussion in Sects 3 and 4 in S1 Text). Thus, I assume that the AARS numbers present in the cell are able to support the maximal ribosome elongation rate possible following a nutrient up-shift.

Fig 5 shows the 12 proteomics data points from [28,32–35] for cysRS and hisRS turnover numbers, which shows a striking amount of variation between experimental groups. The corresponding violin plots have been computed using Eq 8, and the peak can thus be thought of as the most likely value to be observed in an experiment based on the data points and their errors. This analysis provides the ability to pin-point a "consensus" value for the turnover rate as the peak in the violin plot. The red line corresponds to the turnover value that has been used to calculate the number of enzymes via Eq 10 and for the subsequent optimization of k_{cat} values in the next section. Similar plots for the remaining 18 AARS enzymes can be found in Fig F and Fig G in S1 Text.

Finally, Fig 6 shows a comparison of the *in vivo* activity of AARS enzymes (*i.e.* their calculated turnover rates) with experimental *in vitro* measurements of the their k_{cat} values. Black bars indicate the range of *in vivo* activity based on the 12 proteomics data measurements while red bars indicate the range of k_{cat} measurements. In general, there is some level of overlap between the range of *in vivo* turnover rates and *in vitro* k_{cat} measurements for 14 of the enzymes, while 6 (specifically valRS, ileRS, serRS, proRS, thrRS, and alaRS) have measured k_{cat} ranges below their expected *in vivo* turnover rates based on the proteomics data. This suggests that some of the experimental k_{cat} measurements will require a shift upwards in order for the enzyme to support the observed *in vivo* turnover rates.

Optimized k_{cat}, K_m, and tRNA numbers are in reasonable agreement with *in vitro* measurements. We now come to the general problem of reconciling differences between *in vitro* measured aminoacylation k_{cat} values and the observed turnover rates of the enzymes *in vivo*. We must have the situation that the k_{cat} values for the AARS enzymes are strictly greater than

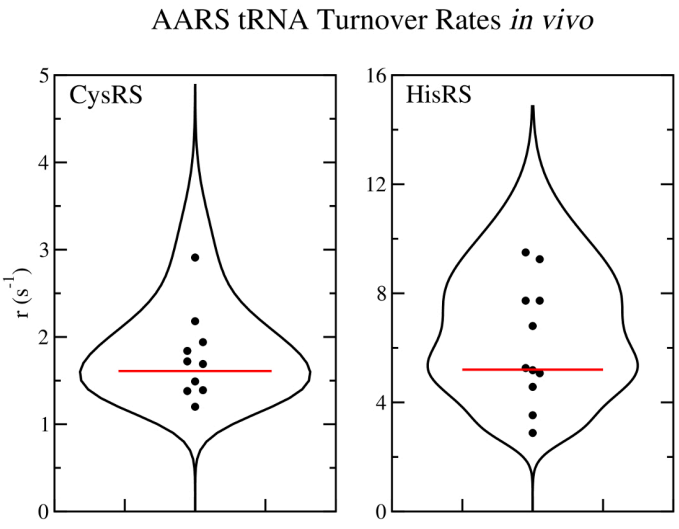

Fig 5. Average tRNA turnover rates *in vivo* for CysRS and HisRS. (A) Violin plot of the average tRNA turnover rates for (A) cysRS and (B) hisRS computed using the 12 proteomics measurements. Red line corresponds to the consensus turnover rate used for computing average enzyme numbers for use in translation simulations.

https://doi.org/10.1371/journal.pcbi.1013353.g005

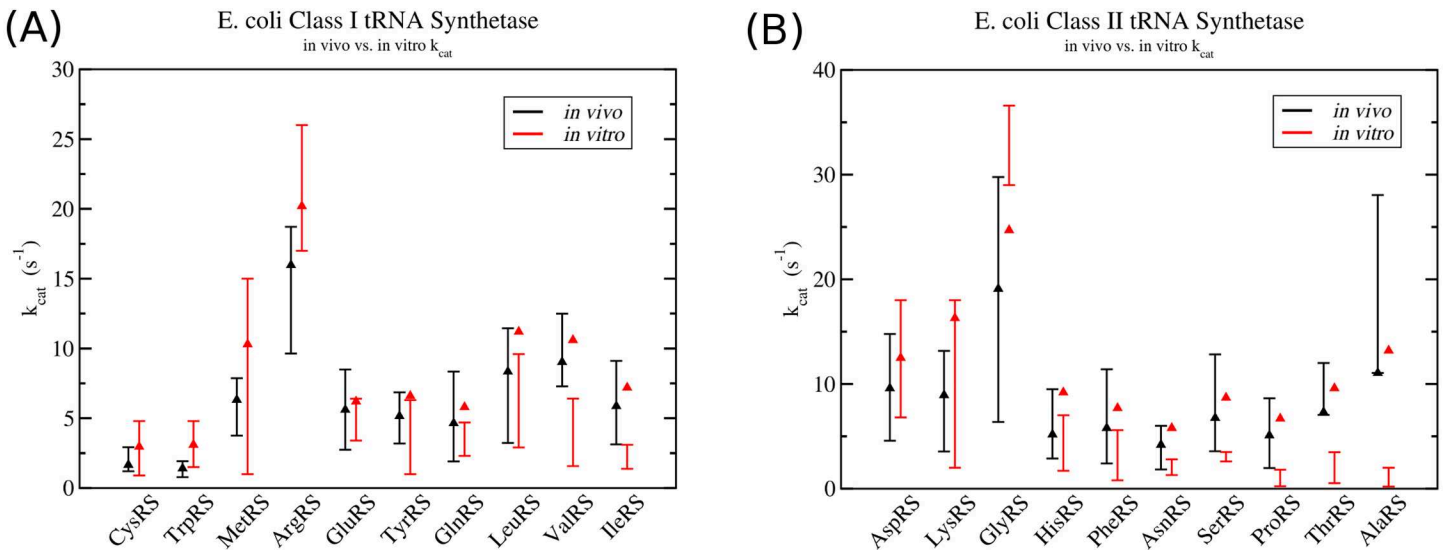

Fig 6. Comparison between *in vivo* activity verses *in vitro* k_{cat} measurements in class I and II aminoacyl tRNA synthetases. Black lines with error bars indicate the range of *in vivo* activity for each AARS enzyme determined from proteomics data, while black triangles give the turnover rate used to calculate the number or enzymes for computational simulations. Red lines with error bars correspond to the range of experimental *in vitro* k_{cat} measurements. Red triangles represent the optimized k_{cat} values which are able to support maximum ribosome elongation rate that would be possible following a nutrient up-shift. Data for (A) class I tRNA synthetases and (B) class II tRNA synthetases.

https://doi.org/10.1371/journal.pcbi.1013353.g006

the *in vivo* turnover rates ($k_{cat} > r$). Based on the data in Fig 6, it is clear that several of the AARS enzymes will require an adjustment to their k_{cat} in order for the enzyme to support the observed *in vivo* turnover rate. To make the adjustments, I follow the procedure outlined in Sect 7 in S1 Text. Essentially, this procedure attempts to minimise the discrepancy between computational simulations of *in vivo* translation and tRNA aminoacylation and several experimental observations. These observations are; the average numbers of each tRNA in the cell, proteomics data on the average number of AARS enzymes, and the percentages of charged tRNA in the cell. See S1 Text for full discussion of the optimization procedure.

The optimized k_{cat} values for all 20 AARS enzymes are shown as red triangles in Fig 6, with the optimised turnover rates shown as black triangles. Optimized turnover rates can be converted to enzyme numbers using Eq 10. Fig 6, along with Fig F and Fig G in S1 Text, reveal that all of the optimized turnover numbers are within the range of experimental proteomics measurements. Moreover, the optimized k_{cat} values in Fig 6 show that 8 of the AARS enzymes (specifically cysRS, trpRS, metRS, argRS, gluRS, tyrRS, aspRS, and lysRS) have optimized k_{cat} values within the range of experimental *in vitro* measurements. The remaining 12 AARS enzymes have optimized k_{cat} values which are above the range of *in vitro* measurements, deviating on average by a factor of 2.08 from the highest measured value. Specific deviation factors are; (valRS - 1.65), (ileRS - 2.32), (leuRS - 1.16), (glnRS - 1.23), (serRS - 2.48), (thrRS - 2.74), (proRS - 3.72), (hisRS - 1.31), (asnRS - 2.07), (alaRS - 6.6), and (pheRS - 1.37). The class I tRNA synthetases have the smallest deviations, while the class II synthetases have the largest, with alaRS and proRS deviating by more than a factor of 3. Some of this deviation maybe explained from macromolecular crowding effects in the cell. Recently Weilandt and Hatzimanikatis have shown that macromolecular crowding can result in an effective increase in k_{cat} by a factor of up to 1.6 [38], which suggests that the small deviations in k_{cat} for hisRS, valRS, glnRS, and leuRS can be potentially explained by this effect. The larger deviations that

are observed in, for instance alaRS, suggests that either the *in vitro* k_{cat} measurements and/or the proteomics measurement of the enzyme abundance in the cell need to be revisited.

The optimized K_m values for both amino acid and tRNA as substrate are shown in Fig 7. Experimental K_m measurements are depicted as violin plots (black lines), with the peak in the violin plot being the most likely value to be observed in an experiment based on the data points and their errors. All of the optimized K_m values, shown as green triangles, fit within the

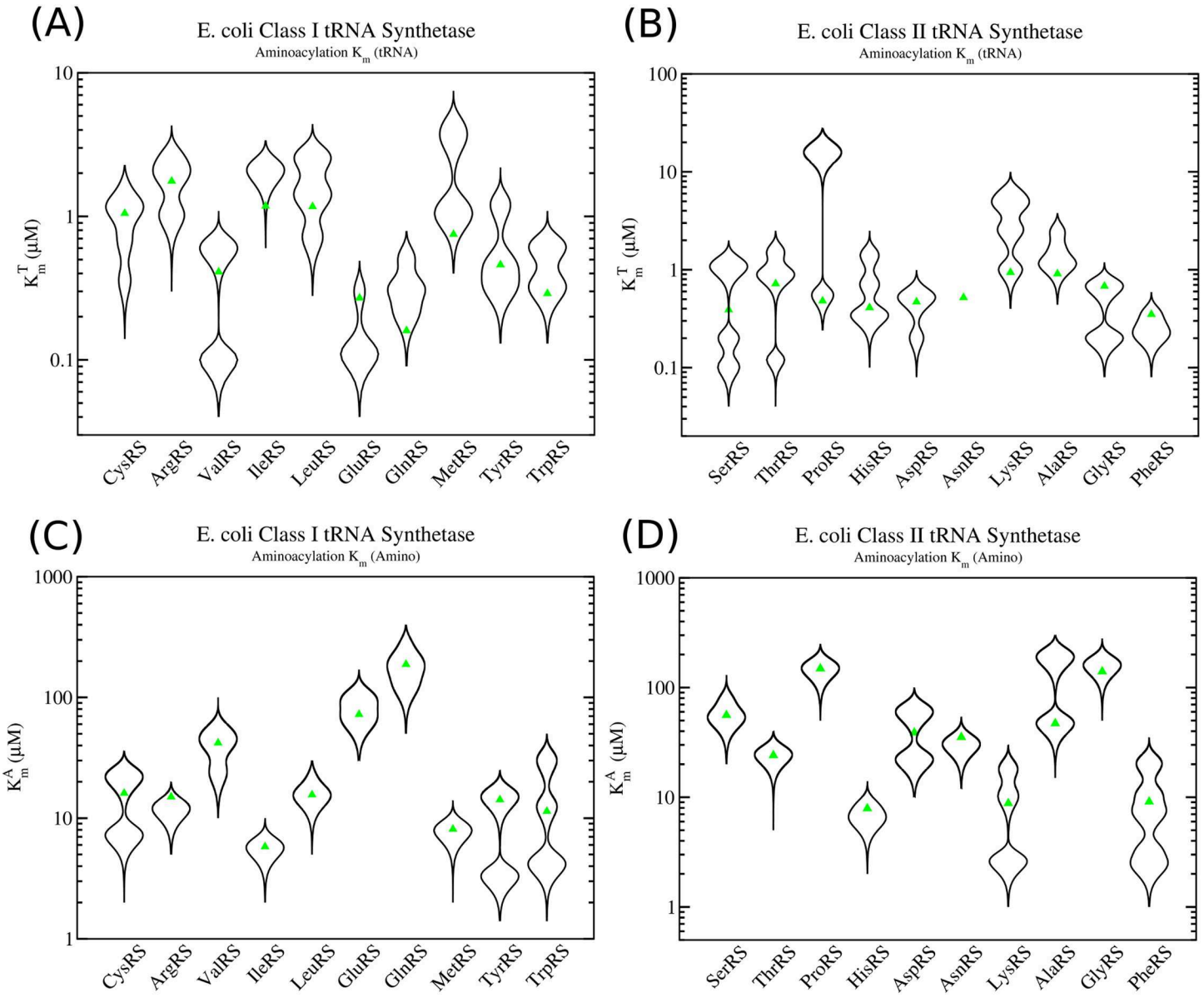

Fig 7. Experimental *in vitro* K_m measurements in class I and class II aminoacyl-tRNA synthetases. Violin plots of the experimental *in vitro* K_m measurements are given as black lines. Green triangles represent the optimized K_m values used in translation simulations. (A) K_m^{trna} values for tRNA as substrate in the aminoacylation reaction for class I enzymes and (B) class II enzymes. (C) K_m^{aa} values for amino acid as substrate in the aminoacylation reaction for class I enzymes and (D) class II enzymes.

https://doi.org/10.1371/journal.pcbi.1013353.g007

ranges of the experimental *in vitro* measurements. Table I in S1 Text summarises the kinetic parameters for each of the enzymes.

Finally, Table G in S1 Text compares the total number of each tRNA isoacceptor used in the model with experimental measurements from Dong et al. [30] for *E. coli* cells growing at $\mu = 0.41$ h^{-1} (doubling time of $\tau = 100$ min). The average absolute error from the values in Dong et al. at this growth rate is 0.3, with the majority of the error coming from only a few tRNAs, specifically metM, his, gln1, gln2, arg3, lys, asn, pro3, and phe. However, when examining the model fit to different growth rates (see Tab H in S2 Spreadsheet S2), one sees that there is sometimes better agreement between the model and the measurements. Taking the minimal absolute error for each tRNA over all growth rates one finds that the error is only 0.18 on average, with the largest errors coming from tRNAs lys, asn, pro3, and phe. Table J in S1 Text gives the optimal tRNA numbers for growth rates of $\mu = 0.41, 0.69, 0.98$ and 1.73 which are used in the full model.

Simulations of *in vivo* tRNA charging kinetics. With optimized k_{cat} and K_m values for the AARS enzymes identified, it now remains to validate that the tRNA charging kinetics of the enzymes can support the translation and tRNA turnover rates observed *in vivo*. I have Incorporated the kinetic reaction scheme for class I and II enzymes (Fig 1) into my stochastic model of translation [26,27] using the kinetic parameters in Tables B, C, and D in S1 Text. The values of k_{cat} and K_m that result from these parameters are shown in Table I in S1 Text. The stochastic model of *in vivo* translational kinetics of *E. coli* in Refs. [26,27] is capable of simulating up to 60k ribosomes on 10k mRNAs and takes into account all known biochemical steps in the translation process. A few examples of features included in the model are; Ef-Tu recharging by Ef-Ts where Ef-Ts binds to Ef-Tu to increase the exchange rate of GDP for GTP, competition between tRNAs for the A-site, stalling between ribosomes on the same mRNA, and initiation, recycling, and termination events on the mRNAs.

Fig 8 shows the charging kinetics of tRNA^{cys} and tRNA^{his} from a simulation of translation *in vivo* at a growth rate of $\mu = 0.69$ h^{-1} with a doubling time of $\tau = 60$ min. At this growth rate, there are roughly 15000 ribosomes and the total nucleotide content in the cell from the mRNA transcriptome is roughly 2×10^6 nucleotides [29]. To insure that the AARS kinetics can support a nutrient up-shift, I simulate translation post nutrient up-shift by using experimental estimates for amino acid concentrations that would be found for a minimal media supplemented with amino acids (see Table H in S1 Text). The simulation of translational dynamics takes part in two stages. The first stage is a constrained initiation of the system, where all tRNAs in the system are charged and mRNAs are slowly added to the system (pre-steady state). This constrained initiation is biologically artificial and is to ensure that the charging demand of the 20 AARS enzymes do not exceed their maximal capacity during initiation of the simulation. After 40 seconds, all mRNAs have been added and the simulation now corresponds to the translational demand that should be observed in exponentially growing *E. coli* with a doubling time of $\tau = 60$ min (steady state). As can be seen in Fig 8, the dynamics of cysRS and hisRS with optimized k_{cat} values of 2.9 and 9.2 s^{-1}, respectively, are sufficient to support ribosome translation at the maximal average elongation rate of 18.6 aa/sec, which occurs at this growth rate post nutrient up-shift. The remaining 18 AARS enzymes, with their k_{cat} values given in Table I in S1 Text, have also been verified to support translational dynamics at these elongation speeds. Finally, all 20 AARS enzymes have been found to support a maximal average elongation speed of 19.1 aa/sec at the highest growth rate used in this study of $\mu = 1.73$ h^{-1}, and are stable for over 30 min of simulation time.

Interestingly, as illustrated in Fig 8C and 8D, a substantial portion of the tRNA remains bound to AARS enzymes in the steady state. When averaged over all the tRNAs, roughly

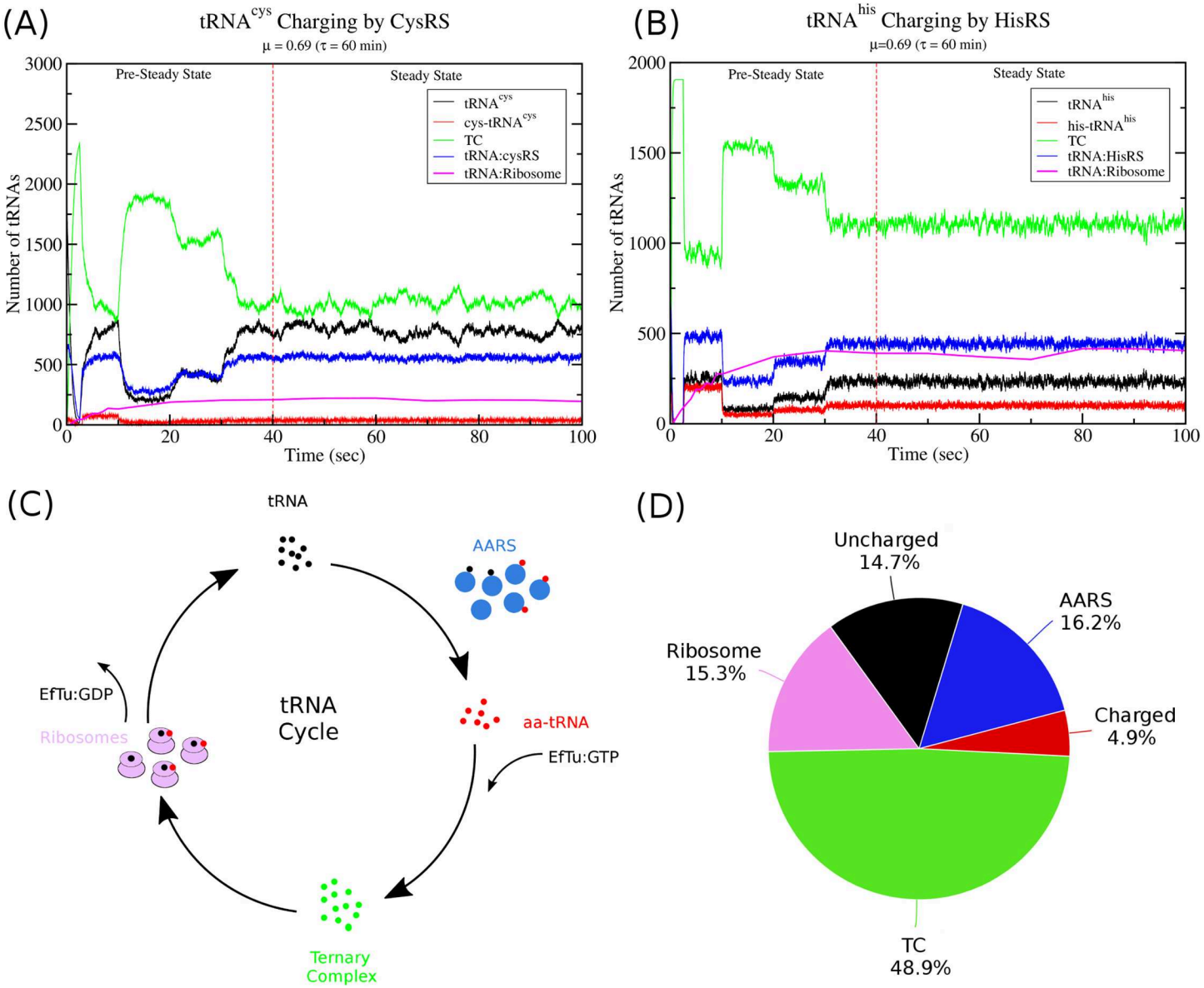

Fig 8. Computational Simulations of tRNA Charging and Translation *in vivo*. (A) The kinetics of $tRNA^{cys}$ charging by cysRS during translation. (B) The kinetics of $tRNA^{his}$ charging by hisRS during translation. (C) The movement of tRNA during the translation cycle. Uncharged tRNAs (black) are charged by AARS enzymes (blue) and released as aa-tRNA (red). The aa-tRNA then binds to EfTu:GTP to form ternary complex (green) which is recruited to the ribosome. Ribosomes (purple) incorporate the amino acid into the peptide chain releasing EfTu:GDP and uncharged tRNAs. (D) Partitioning of the *total* amount of tRNA in the cell. Percentage of total tRNA as free uncharged tRNAs (black), free charged tRNAs (red), free tRNAs in ternary complex (green), and tRNA bound to either ribosomes (purple) or AARS enzymes (blue) is shown as a pie chart at a growth rate of $\mu = 0.69$ ($\tau = 60$ min).

https://doi.org/10.1371/journal.pcbi.1013353.g008

16.2% of the total tRNA in the cell is bound to AARS enzymes either as charged or uncharged tRNAs. This, as we will see in the next section, has important implications for the use of the Michaelis–Menten equation when modelling AARS kinetics.

Effect of intracellular amino acid concentration on translational speed and tRNA charging. It should be noted that I have parametrised the AARS enzyme k_{cat} and K_m values

to ensure that they can support the fastest translational speeds that would occur after a nutrient up-shift in exponentially growing *E. coli* cells. For instance, I calculate the average translational speed of ribosomes in cells with a doubling time of $\tau = 100$ min post nutrient up-shift is roughly 18.0 aa/sec for all mRNAs and 16.2 aa/sec for the LacZ mRNA. These values are quite similar to the average translational speeds of 19.1 and 17.3 aa/sec that I calculate over all mRNAs or the LacZ mRNA at one of the fastest growth rates (doubling time of 24 min), where nutrients are presumed to be plentiful. However, in minimal media with no supplemented amino acids, the average translational speed of the ribosome over all mRNAs have been experimentally estimated to be roughly 15 aa/sec by Bremer and Dennis at a doubling time of 100 min [29]. Dai et al. on the other hand measure the average translational speed of ribosomes on the LacZ mRNA and find values of roughly 12 aa/sec at a cell doubling time of 100 min [36].

To test if my model is capable of recapitulating these lower average ribosome speeds in nutrient poor conditions, I have calculated the average translational speed of ribosomes at the growth rate of $\mu = 0.41$ h^{-1} in minimal media *without* supplemented amino acids. Since *E. Coli* is capable of synthesising all 20 amino acids, the lack of supplied amino acids must presumably result in lower intracellular concentrations of at least some of the 20 amino acids. Experimental measurements of intracellular amino acid concentrations by Bennett et al. [20], as well as Avcilar-Kucukgoze et al. [39], suggest that the amino acids tryptophan, tyrosine, phenylalanine, and serine may be close to the K_M^{aa} values for their enzymes in minimal media conditions. Using the intracellular amino acid concentrations given in Table H in S1 Text, I simulate translation at the growth rate of $\mu = 0.41$ h^{-1} and find that the average translational speed of ribosomes are 13.3 aa/sec averaged over all mRNAs and 12.5 aa/sec averaged over only the LacZ mRNA. Both of these theoretical calculations are in good agreement with measurements from Dai et al. [36].

Finally, I compare the fraction of charged tRNAs predicted by the model and compare with the observations from several experiments [39–42]. For tRNAs with more then one isoacceptor, the averages for each are combined and weighted by the number of each tRNA isoacceptor in the model. As can be seen in Fig 9, there is very good agreement with the experimental observations, with only tRNA^{ile}, tRNA^{his}, tRNA^{asp}, and tRNA^{asn} being outside the range of experimental measurements. Moreover, the results show that the majority of tRNAs are charged between 70% and 90% (blue dashed lines in Fig 9), even at this lower growth rate. A comparison with the results of Avcilar-Kucukgoze et al. [39] by individual isoacceptor is shown in Fig I in S1 Text.

Development of a Michaelis–Menten Model of AARS kinetics

Simulating the full kinetic model of AARS kinetics, as depicted in Fig 1, will usually have substantial computational costs. Because of this, it is often useful to simplify the kinetic model in order to accelerate the computation speed. One of the most popular and highly used models for enzyme kinetics is the Michaelis–Menten model, which allows for the rate product formation to be estimated from the equation

$$v = \frac{V_m[S]}{K_m + [S]}\,. \tag{11}$$

The rate of product formation v depends on the concentration of free substrate $[S]$ and the maximal velocity (or maximal rate of product formation) of the enzyme V_m. The quantity V_m in Eq 11 is related to the total amount of enzyme $[E_0]$ and the enzymes k_{cat} via $V_m = k_{cat}[E_0]$.

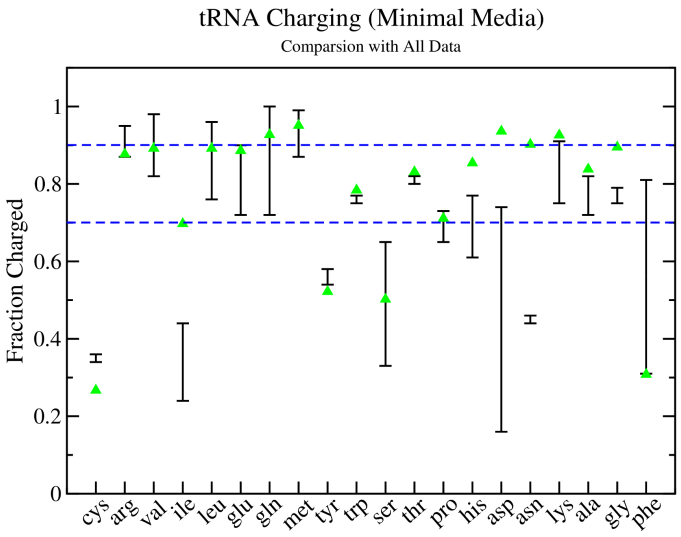

Fig 9. Theoretical and Experimental Estimates of tRNA Charging Fractions in Minimal Media. The total fraction of tRNAs charged in exponentially growing *E. coli* cells. Black lines with error bars indicate the range of experimental measurement from several different experiments [39–42], while green triangles give the results of the stochastic translational model with aminoacyl tRNA synthetase kinetics following the reaction scheme in Fig 1 at a growth rate of $\mu = 0.41\ \mathrm{h}^{-1}$.

https://doi.org/10.1371/journal.pcbi.1013353.g009

The K_m is the Michaelis–Menten constant which can be thought of in simple terms as the concentration of substrate at which the enzyme works at half of V_m. Typically one models the formation of product and loss of substrate using the ODEs

$$\begin{aligned}\frac{d[S]}{dt} &= -v + \cdots \\ \frac{d[P]}{dt} &= +v + \cdots\end{aligned} \tag{12}$$

where the dots denote that there may be additional terms in the ODEs which, for example, model binding of substrate and product to other proteins.

The Michaelis–Menten (MM) model is one of the most popular models for enzyme kinetics due to its simplicity and has been previously used to examine AARS kinetics in a model of *in vivo E. coli* metabolism [10]. However, there are at least two issues when using the MM equation (Eq 11) to model AARS enzyme kinetics. First, there are several substrates (ATP, amino acid, and tRNA) and each of these will impact on the speed of product formation. One potential fix is to say that ATP is saturating, and thus model the velocity using the modified equation [10]

$$v(i) = \frac{V_m[AA]}{K_m^a + [AA]} \frac{\frac{[T_i]}{K_m^t(i)}}{1 + \sum_j^n \frac{[T_j]}{K_m^t(j)}}. \tag{13}$$

This equation accounts for charging of n different tRNA isoacceptors by a single AARS enzyme. For instance, glnRS has two tRNA isoacceptors that it charges (tRNA^{gln1} and tRNA^{gln2}), and $v(i)$ is the rate of charging for tRNA isoacceptor i with free concentration $[T_i]$. The second, and more critical issue, is that there are several assumptions about the enzyme

and substrate that must be true in order for the MM equation to be accurate. The MM equation is typically derived assuming that; (1) the total amount of enzyme is much less than the free concentration of substrate and, (2) the enzyme is present as either free enzyme or a complex of enzyme and substrate. The first condition is clearly violated here, as proteomics data [28,32–35] and measurements of total tRNA concentrations [30] show that the number of AARS enzymes is often similar to the total tRNA numbers. For example, Refs. [28,33] both report around 800 cysRS enzymes at a growth rate of $\mu = 0.69\ h^{-1}$, while Dong et al. measure around 3200 $tRNA^{cys}$. Most of this tRNA will be in ternary complex or charged, and as can be seen from the simulation of the full cysRS kinetic model in the presence of translation in Fig 8A, around 750 $tRNA^{cys}$ are uncharged, similar to the number of cysRS enzymes. Similarly, the second condition is also violated as a substantial amount of aa-tRNA (the product) remains bound to the enzyme during steady state catalysis (cf. Fig 8).

In one sense these are minor issues as I have found that, in general, the AARS enzyme kinetics modelled by the reaction scheme in Fig 1 clearly can be approximated by the MM equation. However potential problems arise when optimising k_{cat} and K_m^{trna} values for a MM model. For example, if the MM model does not correctly account for the amount of tRNA that is bound to the enzyme, then this will result in an over estimation of the quantity of uncharged tRNAs, or tRNAs in ternary complex, etc. as one tries to reconcile the model with the total tRNA measurements from Dong et al. [30]. For example, K_m^{trna} values may need to be increased in order to compensate for the extra uncharged tRNA. There are two approaches that can be used to fit k_{cat}, K_m, and overall tRNA numbers for an MM model; (1) use the tRNA numbers from Dong et al. and adjust k_{cat} and K_m appropriately, or (2) use the K_{cat} and K_m values that have been optimised for the full kinetic reaction scheme in Fig 1 (see Table I in S1 Text for the optimised values) and adjust the tRNA numbers. Since the MM model does not properly account for the amount of charged tRNA product that remains bound to the enzyme, I have taken the latter approach here and adjusted the tRNA numbers to account for this issue.

The final optimised tRNA numbers for various *E. coli* growth rates are given in Table J in S1 Text. This table gives both the optimised tRNA numbers for the MM model as well as for the full kinetic reaction scheme shown in Fig 1. As can be seen, there is a reduction in the number of tRNAs for the MM model compared to the full kinetic model. This illustrates that the full kinetics of AARS enzymes, as well as the status and location of the tRNAs (*i.e.* are they bound to AARS, bound to ribosome, or in free ternary complex), need to be accounted for in order to correctly compare with the experimental tRNA numbers from Dong et al. [30]. Details of the amount of tRNA that is bound to ribosome and is present in ternary complex used for the fitting of the full model can be found in Tab H in S1 Spreadsheet.

Discussion

I have developed an empirical kinetic model for all 20 tRNA synthetase enzymes from *E. coli*, where the individual binding and catalytic events that take place in the aminoacylation process are explicitly considered. Model predictions for each of the 20 kinetic models have been validated and shown to support steady state translational kinetics in an average cell undergoing exponential growth with doubling times of τ = 100, 60, 40, and 24 min. The resulting optimised k_{cat} values are in reasonable agreement with *in vitro* k_{cat} measurements, with 8 out of 20 AARS enzymes having optimized values within the ranged observed in experiments. The remaining 12 AARS have optimised k_{cat} which deviate from experiment by only a factor of 2 on average. Likewise, the optimized Michaelis–Menten constants for amino acid and tRNA (K_m^{aa} and K_m^{trna}) are also within experimental ranges for all 20 AARS enzymes

(cf. Fig 7). Despite these results, it is still important to note that the kinetic parameters and overall reaction scheme for the aminoacylation model depicted in Fig 1 should not be considered as definitive, but instead should be thought of as a starting point for refinements as further experimental data are obtained in future. For instance, the model currently assume the highest measured values for intracellular concentrations of AMP and PPi of 250 and 500 μM, respectively. However, it is possible that the concentrations of these metabolites are actually much lower in the cell. If this was to be confirmed experimentally, it would enable a further lowering of k_{cat} values in the model since both AMP and PPi are predicted by the model to be inhibitors of aminoacylation. Regardless, several important conclusions can be drawn based on these empirical kinetic models.

One of the important conclusions from the analysis of this work is that the total tRNA in the cell is partitioned as free uncharged/charged tRNA as well as bound tRNA, and that a substantial fraction (approximately 16% of the total tRNA) remains bound to AARS enzymes during steady state translation. Dong et al. [30] have previously noted that while the amount of tRNA in ternary complex required for optimal elongation rate should be proportional to the square root of the codon frequency (see Sect 4 in S1 Text), the total tRNA abundances measured roughly scale with the square of the codon frequency. By taking into account the number of tRNAs bound to the ribosome, Dong et al. showed that the resulting total tRNA abundances more closely fit to the square of the codon frequency. However, they assumed that tRNA was only either in free ternary complex or bound to ribosomes. Based on the kinetic model in Fig 1, I have shown that the fraction of charged and uncharged tRNA that is bound to AARS enzymes will likely also represent a substantial portion of the total tRNA. This has important consequences for the fitting of parameters for Michaelis–Menten models of AARS kinetics and their subsequent validation with experimental observations as discussed in the results.

A second conclusion is that most of the *in vitro* experimental measurements of k_{cat} and K_m values are fairly close to what are needed to support the estimated tRNA aminoacylation rates in the cell. In this work, I have found that 8 out of the 20 AARS enzymes (cysRS, trpRS, metRS, argRS, gluRS, tyrRS, aspRS, and lysRS) have *in vitro* measured k_{cat} values which are within the range of expected turnover rates determined by proteomics measurements (cf. Fig 6). The remaining 12 AARS enzymes have optimised k_{cat} values which deviate on average by a factor of 2 from experimental *in vitro* measurements. This is in contrast to recent work by Choi and Convert [10] which parameterised a Michaelis–Menten model of AARS kinetics for all 20 AARS enzymes and found that their optimised values deviated from *in vitro* k_{cat} measurements on average by roughly a factor of 7 [10]. There are several reasons for the discrepancy with my work here.

First, Choi and Covert do not seem to distinguish between the k_{cat} for aminoacylation versus that for pyrophosphate exchange. For example, the k_{cat} for pyrophosphate exchange for cysRS (see Table 1) tends to be measured around 90 s^{-1}, about 30 times faster than the k_{cat} measurements for aminoacylation (around 2.9 s^{-1}). Instead, their fitting procedure appears to consider both values when optimising the aminoacylation k_{cat}. It is important to note that the pyrophosphate exchange k_{cat} is measuring the exchange of ATP and pyrophosphate on an adenylate bound enzyme. Thus, it is a proxy for the rate of the first catalytic event, *i.e.* activation of the amino acid. In contrast, the aminoacylation k_{cat} measures the entire process of amino acid activation plus transfer of the amino acid to the tRNA and is the only one that has a relation to the measured *in vivo* turnover rates. Their higher reported aminoacylation k_{cat} for cysRS (69.44 s^{-1} [10]) is potentially due to their fitting algorithm being allowed to search up to 90 s^{-1}. As a result, they report a factor of ≈ 3 deviation from an experimental

average of 23.1 ± 35.9 s^{-1}, where this average includes the pyrophosphate exchange k_{cat} measurements. Comparing to only experimental aminoacylation k_{cat} values in Table 1, the value 69.44 deviates from the average of 2.96 s^{-1} by over a factor of 23.

Second, there seems to be a substantial difference between AARS numbers that I have calculated here versus what Choi and Covert have calculated. To calculate AARS numbers, Choi and Covert use their Parca *E. coli* model [43] to estimate protein numbers in the cell. They then compare the average protein numbers with those from Schmidt et al. [34] and with single cell proteomics data from Taniguchi et al. [31]. Next, they estimate amino acid usage in the cell by calculating the number of proteins to be doubled, and use the codon composition of the protein's mRNA and doubling time of the cell to determine the codon reading rate for each codon. In contrast, I have used averaged proteomics data from 12 different measurements to estimate consensus AARS numbers and have used my ribosome translational model which simulates translation on the full transcriptome in the cell to estimate amino acid usage. My transcriptome was constructed using mRNA-seq measurements from Li et al. [28] (see Methods) to estimate the number of each mRNA present in the cell. Remarkably, we are both in very good agreement on the amino acid usage / codon reading rates. Choi and Covert report for *E. coli* with ≈ 26000 ribosomes in minimal media supplemented with amino acids a usage rate for the amino acid cysteine of 4.478 μM s^{-1} (or 2696.6 s^{-1} in the average cell volume of 1 μm^3 at this growth rate). I find a very similar result using a transcriptome based on mRNA-seq data from Li et al. [28] of 4.508 μM s^{-1} (or 2714.8 s^{-1}). Despite the good agreement on amino acid usage rates, we substantially differ on AARS numbers. For example, I have calculated an optimal value of 1610 enzymes for cysRS, similar to the 1409 measured by Mori et al. [33] for bacteria with a growth rate of approximately $\mu = 1.04$ h^{-1}. In contrast, Choi and Covert estimate 606 on average at a very similar growth rate [10]. As a result, my average turnover rate for cysRS is 1.68 s^{-1} versus 4.44 s^{-1} for Choi and Covert, roughly 3 times lower. There is a similar trend over the remaining AARS enzymes (see Table K in S1 Text). Choi and Covert report that, since their simulation of average protein numbers from the Parca model are within a factor of 10 from Schmidt et al. [34] and had a coefficient of determination of $R^2 = 0.63$, there was satisfactory agreement with the measured proteome values of Schmidt et al. [10]. However, as Fig 5 shows, if we perform a meta analysis by including additional proteomics measurements from several different groups, we see that there is substantial variation amongst these measurements. Although this suggests that relying on a single proteomics data point may be potentially problematic, a consensus value does seem to emerge when weighted over multiple measurements from different groups.

Finally, Choi and Covert report optimised values of $k_{cat} = 69.44$ s^{-1} and $K_m^{trna} = 10.6$ μM for cysRS [10]. This is in contrast to the optimised values that I find here of $k_{cat} = 2.9$ s^{-1} and $K_m^{trna} = 1.05$ μM. Given Choi and Covert's estimated turnover rate of $r = 4.44$ s^{-1} for cysRS, one can solve for the amount of free uncharged tRNA in their model using the MM equation (Eq 11) and find $[T_u] = 0.724$ μM. Thus in a quasi-steady state, their translational model with a MM model of aminoacylation should have each cysRS enzyme averaging a turnover of 4.44 tRNAs per second, with a free concentration of uncharged $tRNA^{cys}$ of 0.724 μM in the cell. But in the Michaelis–Menten model, k_{cat} and K_m^{trna} satisfy the relation

$$k_{cat} = \frac{r}{[T_u]} K_m^{trna} + r\,. \tag{14}$$

This relation implies that, given the enzyme turnover rate r and the amount of free uncharged tRNA $[T_u]$, a re-scaling of k_{cat} and K_m^{trna} is possible. This re-scaling procedure does

not seem to have been applied in their fitting procedure, or it was applied to values that incorrectly included the pyrophosphate exchange k_{cat} values, which tend to be an order of magnitude higher. For example, applying this re-scaling to Choi and Covert's cysRS parameters, one can obtain new values of $k_{cat} = 8.36\ s^{-1}$ and $K_m^{trna} = 0.64\ \mu M$, which are much closer to the two experimental *in vitro* measurements of $k_{cat} = 4.8\ s^{-1}$ and $K_m^{trna} = 0.64\ \mu M$ reported in Table 1.

In summary, the models I have developed here provide a basis for examining tRNA charging that occurs *in vivo* by aminoacyl tRNA synthetases in *E. coli* cells. The analysis has revealed that for 8 out of the 20 AARS enzymes, the *in vitro* measurements of k_{cat} and K_m^{trna} are in line with the enzyme turnover rates that would be expected *in vivo* based on average proteomics measurements, with the remaining 12 requiring a small adjustment by a factor of 2 on average. However, a few class II enzymes, in particular, serRS, thrRS, proRS, and alaRS, deviate more substantially. More experimental data will be needed to elucidate the origin of this discrepancy, and refine the kinetic models appropriately in these cases. Regardless, the models I report on here should hopefully be an important tool for the community to theoretically investigate, for example, the effects of amino acid supply on the cellular translational machinery in bacteria. Moreover, they present a new opportunity to explore the energy charge model of Brenner et al. [44], or model the effects of tRNA over-expression as potential therapies for Charcot-Marie-Tooth disease [45].

Supporting information

S1 Spreadsheet.
(XLSX)

S1 Text.
(PDF)

Fig A. Kinetic reaction scheme for the pyrophosphate exchange reaction. State S_0 represents the AARS enzyme, while S_1 and S_2 are the amino acid and ATP bound enzymes, respectively. State S_3 is the enzyme with both amino acid and ATP bound, S_4 is the adenylate and pyrophosphate bound state, while state S_5 is the adenylate bound enzyme state.

Fig B. Effect of parameter variation on pyrophosphate exchange kinetics. (A-C) Effect on Michaelis–Menten constant K_m and pyrophosphate k_{cat} as the amino acid and ATP dissociation constant is varied. (D-F) Effect on the Michaelis–Menten constant K_m and pyrophosphate k_{cat} as the amino acid activation rates k_{5f} and k_{5b} are varied. (G-I) Effect on the Michaelis–Menten constant K_m and pyrophosphate k_{cat} as the pyrophosphate release rates k_{6f} and k_{6b} are varied.

Fig C. Kinetic reaction scheme for Class I aminoacyl tRNA synthetases. Reaction scheme diagram labelling the individual kinetic reactions in the aminoacylation reaction for the class I aminoacyl tRNA synthetase enzymes. Individual kinetic rates for each reaction can be found in Table B. The states of the enzyme S_i are given in the legend on the right with abbreviations E = AARS enzyme, T = ATP, M = AMP, P = PP_i, D = AA Adenylate, R = tRNA, and R* = AA-tRNA denoting the charged tRNA. For example, state S_0 corresponds to the enzyme free of all substrates while S_5 corresponds to the enzyme with bound amino acid adenylate.

Fig D. Kinetic reaction scheme for Class II aminoacyl tRNA synthetases. Reaction scheme diagram labelling the individual kinetic reactions in the aminoacylation reaction for the class II aminoacyl tRNA synthetase enzymes. Individual kinetic rates for each reaction can be found in Tables C and D. The states of the enzyme S_i are given in the legend on the right with abbreviations E = AARS enzyme, T = ATP, M = AMP, P = PP_i, D = AA Adenylate, R =

tRNA, and R* = AA-tRNA denoting the charged tRNA. For example, state S_0 corresponds to the enzyme free of all substrates while S_5 corresponds to the enzyme with bound amino acid adenylate. States with substrate bound in the first and second site are separated by a slash, *e.g.* state S_{15} with charged tRNA in the first site and AA is bound to the second catalytic site is denoted as ER*/A.

Fig E. The dependence of the translation elongation rate on total ternary complex concentration. Stochastic simulations of translation *in vivo* are used to calculate the average elongation rate of ribosomes in *E. coli* for different cellular volumes verses the percentage of the total amount of tRNA in ternary complex. The fractions of each tRNA isoacceptor in ternary complex set to the optimal values listed in Table G (see section 4 for further details).

Fig F. Estimated average tRNA turnover rates for class I aminoacyl tRNA synthetases. Violin plots for the AARS tRNA turnover rates are shown for each of the class I enzymes, with cysRS shown in Fig 5 of the main text. Each of the individual proteomics data points used to construct the violin plot are shown (black dots) along with the value used for optimization (red line).

Fig G. Estimated average tRNA turnover rates for class II aminoacyl tRNA synthetases. Violin plots for the AARS tRNA turnover rates are shown for each of the class II enzymes, with hisRS shown in Fig 5 of the main text. Each of the individual proteomics data points used to construct the violin plot are shown (black dots) along with the value used for optimization (red line).

Fig H. Average tRNA usage rates for the three proline tRNA isoacceptors. Theoretical average tRNA usage rates for $tRNA^{pro1}$ (black line), $tRNA^{pro2}$ (red line) and $tRNA^{pro3}$ (green line) are shown using a fixed ratio of $tRNA^{pro2}$ to $tRNA^{pro3}$ of y = 1.25 in ternary complex. The graph is plotted as a function of the ratio of $tRNA^{pro1}$ to $tRNA^{pro3}$ in ternary complex.

Fig I. Theoretical and Experimental Estimates of tRNA Charging Fractions in Minimal Media. The total fraction of tRNAs charged in exponentially growing *E. coli* cells. Black lines with error bars indicate the range of experimental measurement from Avcilar-Kucukgoze et al. [39], while green triangles give the results of the stochastic translational model with aminoacyl tRNA synthetase kinetics following the reaction scheme in Fig C and Fig D at a growth rate of $\mu = 0.41\ h^{-1}$.

Table A. Classification and Properties of Aminoacyl tRNA Synthetases from *E. coli*. For each of the 23 genes encoding an aminoacyl tRNA synthetase, the class, number of subunits which make up the functional enzyme, and if the enzyme has been observed to have burst kinetics or editing, is shown.

Table B. Kinetic parameters for Class I aminoacyl tRNA synthetase models. Labels of the reactions correspond to those shown in Fig C.

Table C. Kinetic parameters for Class II aminoacyl tRNA synthetase models. Part 1 of 2. Labels of the reactions correspond to those shown in Fig D.

Table D. Kinetic parameters for Class II aminoacyl tRNA synthetase models. Part 2 of 2. Labels of the reactions correspond to those shown in Fig D.

Table E. Estimates of AARS Activity *in vivo*. For each of the AARS enzymes, the activity (i.e. tRNA turnover rate r) of a single enzyme is estimated in *E. coli* cells growing at $\mu = 0.69\ h^{-1}$ based on amino acid usage and the number of AARS. Amino acid usage for the Mori et al. data [33] was calculated computationally using a model of *in vivo* translation [26] and

the fractional amount of tRNAs in ternary complex needed for optimal translation, while the amino acid usage for Jakubowski was taken from their experimental amino acid radiolabelling measurements [46].

Table F. Average Number of Proteins, tRNA, and Ribosomes in *E. coli* Cells at Different Growth Rates. Protein numbers are taken from proteome measurements from several groups [28,32,33] and reported here as number per cell. The specific data for each growth rate are; $\mu = 0.41\ h^{-1}$ Valgepea et al. 2013 [32], $\mu = 0.69\ h^{-1}$ and $\mu = 1.04\ h^{-1}$ Mori et al. 2021 [33], $\mu = 1.98\ h^{-1}$ Li et al. 2014 [28]. The number of tRNA and Ribosomes (per cell) are taken from Dennis and Bremer [29]. The doubling time in minutes is computed from the growth rate using $\tau = 60\ln(2)/\mu$.

Table G. Average number of tRNAs per cell and their codon recognition. Data for the number of tRNAs that are in free ternary complex at a growth rate of $\mu = 0.41\ h^{-1}$ ($\tau = 100$ min). The numbers that give the optimal translation rate have been computed from Eq 3 and the procedure outlined in section 4, and the total tRNA numbers are taken from Dong et al. [30]. The values used in the model are the result of the fitting procedure in section 7.

Table H. Concentrations of Amino Acids in *E. coli*. Experimental measurements of intracellular amino acid concentrations are shown for Bennett et al. [20], and minimal media (MM) and minimal media plus amino acids (MM+AA) from Avcilar-Kucukgoze [39]. The values used in the model for the MM+AA scenario is shown in the final column. (n.d. = not determined).

Table I. Optimized numbers of Aminoacyl tRNA Synthetases in Exponentially Growing *E. coli* and optimized k_{cat} and K_m values. The optimized average number of AARS enzymes are shown for different growth rates, $\mu = 0.41\ h^{-1}$ ($\tau = 100$ min), $\mu = 0.69\ h^{-1}$ ($\tau = 60$ min), $\mu = 1.04\ h^{-1}$ ($\tau = 40$ min), and $\mu = 1.73\ h^{-1}$ ($\tau = 24$ min). Corresponding optimized k_{cat} and Michaelis–Menten parameters for tRNA (K_m^t) and amino acid (K_m^a) are given in the right hand columns.

Table J. Optimized numbers of tRNAs per cell and their codon recognition. The optimized total tRNA numbers are shown for the Michaelis–Menten model and the full kinetic model where AARS enzymes are modelled as having reaction scheme according to Fig C for Class I enzymes or Fig D for class II enzymes.

Table K. Model predictions of AARS Activity *in vivo*. For each of the AARS enzymes, the activity (i.e. tRNA turnover rate) of a single enzyme r per second is estimated in *E. coli* cells growing at $\mu = 1.04\ h^{-1}$ ($\tau = 40$ min) based on amino acid usage and the number of AARS. Amino acid usage for the data in this work was calculated computationally using a model of *in vivo* translation [26], while the amino acid usage and AARS numbers for Choi and Covert were taken from supplementary material Tables 8 and S3 [10].

Author contributions

Conceptualization: Eric C. Dykeman.

Data curation: Eric C. Dykeman.

Formal analysis: Eric C. Dykeman.

Investigation: Eric C. Dykeman.

Methodology: Eric C. Dykeman.

Project administration: Eric C. Dykeman.

Resources: Eric C. Dykeman.

Software: Eric C. Dykeman.

Validation: Eric C. Dykeman.

Visualization: Eric C. Dykeman.

Writing – original draft: Eric C. Dykeman.

Writing – review & editing: Eric C. Dykeman.

References

1. Berg P. Studies on the enzymatic utilization of amino acyl adenylates: the formation of adenosine triphosphate. Journal of Biological Chemistry. 1958;233(3):601–7.
2. Fersht AR, Jakes R. Demonstration of two reaction pathways for the aminoacylation of tRNA. Application of the pulsed quenched flow technique. Biochemistry. 1975;14(15):3350–6. https://doi.org/10.1021/bi00686a010 PMID: 1096942
3. Francklyn CS, First EA, Perona JJ, Hou Y-M. Methods for kinetic and thermodynamic analysis of aminoacyl-tRNA synthetases. Methods. 2008;44(2):100–18. https://doi.org/10.1016/j.ymeth.2007.09.007 PMID: 18241792
4. Giegé R, Springer M. Aminoacyl-tRNA synthetases in the bacterial world. EcoSal Plus. 2016;7(1):10.1128/ecosalplus.ESP-0002–2016. https://doi.org/10.1128/ecosalplus.ESP-0002-2016 PMID: 27223819
5. Rubio Gomez MA, Ibba M. Aminoacyl-tRNA synthetases. RNA. 2020;26(8):910–36. https://doi.org/10.1261/rna.071720.119 PMID: 32303649
6. Airas RK. Kinetic analysis of the isoleucyl-tRNA synthetase mechanism: the next reaction cycle can start before the previous one ends. FEBS Open Bio. 2017;8(2):244–55. https://doi.org/10.1002/2211-5463.12362 PMID: 29435414
7. Airas RK. Analysis of the kinetic mechanism of arginyl-tRNA synthetase. Biochim Biophys Acta. 2006;1764(2):307–19. https://doi.org/10.1016/j.bbapap.2005.11.020 PMID: 16427818
8. Santra M, Bagchi B. Catalysis of tRNA aminoacylation: single turnover to steady-state kinetics of tRNA synthetases. J Phys Chem B. 2012;116(39):11809–17. https://doi.org/10.1021/jp305045w PMID: 22957855
9. Zhang CM, Perona JJ, Ryu K, Francklyn C, Hou YM. Distinct kinetic mechanisms of the two classes of aminoacyl-tRNA synthetases. Journal of Molecular Biology. 2006;361(2):300–11.
10. Choi H, Covert MW. Whole-cell modeling of E. coli confirms that in vitro tRNA aminoacylation measurements are insufficient to support cell growth and predicts a positive feedback mechanism regulating arginine biosynthesis. Nucleic Acids Research. 2023;51(12):5911–30.
11. Sun G, Ahn-Horst TA, Covert MW. The E. coli whole-cell modeling project. EcoSal Plus. 2021;9(2):eESP00012020. https://doi.org/10.1128/ecosalplus.ESP-0001-2020 PMID: 34242084
12. Dittmar KA, Sørensen MA, Elf J, Ehrenberg M, Pan T. Selective charging of tRNA isoacceptors induced by amino-acid starvation. EMBO reports. 2005;6(2):151–7.
13. Elf J, Ehrenberg M. Near-critical behavior of aminoacyl-tRNA pools in E. coli at rate-limiting supply of amino acids. Biophys J. 2005;88(1):132–46. https://doi.org/10.1529/biophysj.104.051383 PMID: 15501947
14. Fersht AR, Kaethner MM. Mechanism of aminoacylation of tRNA. Proof of the aminoacyl adenylate pathway for the isoleucyl- and tyrosyl-tRNA synthetases from Escherichia coli K12. Biochemistry. 1976;15(4):818–23. https://doi.org/10.1021/bi00649a014 PMID: 764868
15. Jakes R, Fersht AR. Tyrosyl-tRNA synthetase from Escherichia coli. Stoichiometry of ligand binding and half-of-the-sites reactivity in aminoacylation. Biochemistry. 1975;14(15):3344–50.
16. Xiang M, Xia K, Chen B, Luo Z, Yu Y, Jiang L, et al. An asymmetric structure of bacterial TrpRS supports the half-of-the-sites catalytic mechanism and facilitates antimicrobial screening. Nucleic Acids Res. 2023;51(9):4637–49. https://doi.org/10.1093/nar/gkad278 PMID: 37070195
17. Guth EC, Francklyn CS. Kinetic discrimination of tRNA identity by the conserved motif 2 loop of a class II aminoacyl-tRNA synthetase. Mol Cell. 2007;25(4):531–42. https://doi.org/10.1016/j.molcel.2007.01.015 PMID: 17317626

18. Pope AJ, Lapointe J, Mensah L, Benson N, Brown MJ, Moore KJ. Characterization of isoleucyl-tRNA synthetase from Staphylococcus aureus. I: Kinetic mechanism of the substrate activation reaction studied by transient and steady-state techniques. J Biol Chem. 1998;273(48):31680–90. https://doi.org/10.1074/jbc.273.48.31680 PMID: 9822629
19. Kern D, Lapointe J. The catalytic mechanism of glutamyl-tRNA synthetase of Escherichia coli. Evidence for a two-step aminoacylation pathway, and study of the reactivity of the intermediate complex. Eur J Biochem. 1980;106(1):137–50. PMID: 6280993
20. Bennett BD, Kimball EH, Gao M, Osterhout R, Van Dien SJ, Rabinowitz JD. Absolute metabolite concentrations and implied enzyme active site occupancy in Escherichia coli. Nat Chem Biol. 2009;5(8):593–9. https://doi.org/10.1038/nchembio.186 PMID: 19561621
21. Kukko E, Heinonen J. The intracellular concentration of pyrophosphate in the batch culture of Escherichia coli. European Journal of Biochemistry. 1982;127(2):347–9.
22. Kukko-Kalske E, Lintunen M, Inen MK, Lahti R, Heinonen J. Intracellular PPi concentration is not directly dependent on amount of inorganic pyrophosphatase in Escherichia coli K-12 cells. J Bacteriol. 1989;171(8):4498–500. https://doi.org/10.1128/jb.171.8.4498-4500.1989 PMID: 2546923
23. Hélène C, Brun F, Yaniv M. Fluorescence studies of interactions between Escherichia coli valyl-tRNA synthetase and its substrates. J Mol Biol. 1971;58(1):349–56. https://doi.org/10.1016/0022-2836(71)90251-8 PMID: 4932655
24. Bovee ML, Pierce MA, Francklyn CS. Induced fit and kinetic mechanism of adenylation catalyzed by Escherichia coli threonyl-tRNA synthetase. Biochemistry. 2003;42(51):15102–13. https://doi.org/10.1021/bi0355701 PMID: 14690420
25. Cole FX, Schimmel PR. On the rate law and mechanism of the adenosine triphosphate–pyrophosphate isotope exchange reaction of amino acyl transfer ribonucleic acid synthetases. Biochemistry. 1970;9(3):480–9. https://doi.org/10.1021/bi00805a005 PMID: 4313472
26. Dykeman EC. A stochastic model for simulating ribosome kinetics in vivo. PLoS Comput Biol. 2020;16(2):e1007618. https://doi.org/10.1371/journal.pcbi.1007618 PMID: 32049979
27. Dykeman EC. Modelling ribosome kinetics and translational control on dynamic mRNA. PLoS Comput Biol. 2023;19(1):e1010870. https://doi.org/10.1371/journal.pcbi.1010870 PMID: 36689464
28. Li G-W, Burkhardt D, Gross C, Weissman JS. Quantifying absolute protein synthesis rates reveals principles underlying allocation of cellular resources. Cell. 2014;157(3):624–35. https://doi.org/10.1016/j.cell.2014.02.033 PMID: 24766808
29. Bremer H, Dennis PP. Modulation of chemical composition and other parameters of the cell at different exponential growth rates. EcoSal Plus. 2008;3(1):10.1128/ecosal.5.2.3. https://doi.org/10.1128/ecosal.5.2.3 PMID: 26443740
30. Dong H, Nilsson L, Kurland CG. Co-variation of tRNA abundance and codon usage in Escherichia coli at different growth rates. Journal of Molecular Biology. 1996;260(5):649–63.
31. Taniguchi Y, Choi PJ, Li G-W, Chen H, Babu M, Hearn J, et al. Quantifying E. coli proteome and transcriptome with single-molecule sensitivity in single cells. Science. 2010;329(5991):533–8. https://doi.org/10.1126/science.1188308 PMID: 20671182
32. Valgepea K, Adamberg K, Seiman A, Vilu R. Escherichia coli achieves faster growth by increasing catalytic and translation rates of proteins. Mol Biosyst. 2013;9(9):2344–58. https://doi.org/10.1039/c3mb70119k PMID: 23824091
33. Mori M, Zhang Z, Banaei-Esfahani A, Lalanne J-B, Okano H, Collins BC, et al. From coarse to fine: the absolute Escherichia coli proteome under diverse growth conditions. Mol Syst Biol. 2021;17(5):e9536. https://doi.org/10.15252/msb.20209536 PMID: 34032011
34. Schmidt A, Kochanowski K, Vedelaar S, Ahrné E, Volkmer B, Callipo L, et al. The quantitative and condition-dependent Escherichia coli proteome. Nat Biotechnol. 2016;34(1):104–10. https://doi.org/10.1038/nbt.3418 PMID: 26641532
35. Peebo K, Valgepea K, Maser A, Nahku R, Adamberg K, Vilu R. Proteome reallocation in Escherichia coli with increasing specific growth rate. Mol Biosyst. 2015;11(4):1184–93. https://doi.org/10.1039/c4mb00721b PMID: 25712329
36. Dai X, Zhu M, Warren M, Balakrishnan R, Patsalo V, Okano H, et al. Reduction of translating ribosomes enables Escherichia coli to maintain elongation rates during slow growth. Nat Microbiol. 2016;2:16231. https://doi.org/10.1038/nmicrobiol.2016.231 PMID: 27941827
37. Brunschede H, Dove TL, Bremer H. Establishment of exponential growth after a nutritional shift-up in Escherichia coli B/r: accumulation of deoxyribonucleic acid, ribonucleic acid, and protein. J Bacteriol. 1977;129(2):1020–33. https://doi.org/10.1128/jb.129.2.1020-1033.1977 PMID: 320174
38. Weilandt DR, Hatzimanikatis V. Particle-based simulation reveals macromolecular crowding effects on the michaelis-menten mechanism. Biophys J. 2019;117(2):355–68. https://doi.org/10.1016/j.bpj.2019.06.017 PMID: 31311624

39. Avcilar-Kucukgoze I, Bartholomäus A, Cordero Varela JA, Kaml RFX, Neubauer P, Budisa N. Discharging tRNAs: a tug of war between translation and detoxification in Escherichia coli. Nucleic Acids Research. 2016;44(17):8324–34.
40. Yegian CD, Stent GS, Martin EM. Intracellular condition of Escherichia coli transfer RNA. Proc Natl Acad Sci U S A. 1966;55(4):839–46. https://doi.org/10.1073/pnas.55.4.839 PMID: 5327069
41. Sørensen MA. Charging levels of four tRNA species in Escherichia coli Rel(+) and Rel(-) strains during amino acid starvation: a simple model for the effect of ppGpp on translational accuracy. J Mol Biol. 2001;307(3):785–98. https://doi.org/10.1006/jmbi.2001.4525 PMID: 11273701
42. Krüger MK, Sørensen MA. Aminoacylation of hypomodified tRNAGlu in vivo. J Mol Biol. 1998;284(3):609–20. https://doi.org/10.1006/jmbi.1998.2197 PMID: 9826502
43. Macklin DN, Ahn-Horst TA, Choi H, Ruggero NA, Carrera J, Mason JC, et al. Simultaneous cross-evaluation of heterogeneous E. coli datasets via mechanistic simulation. Science. 2020;369(6502):eaav3751. https://doi.org/10.1126/science.aav3751 PMID: 32703847
44. Brenner M, De Lorenzo F, Ames BN. Energy charge and protein synthesis. Control of aminoacyl transfer ribonucleic acid synthetases. J Biol Chem. 1970;245(2):450–2. PMID: 4904484
45. Zuko A, Mallik M, Thompson R, Spaulding EL, Wienand AR, Been M, et al. tRNA overexpression rescues peripheral neuropathy caused by mutations in tRNA synthetase. Science. 2021;373(6559):1161–6. https://doi.org/10.1126/science.abb3356 PMID: 34516840
46. Jakubowski H, Goldman E. Quantities of individual aminoacyl-tRNA families and their turnover in Escherichia coli. J Bacteriol. 1984;158(3):769–76. https://doi.org/10.1128/jb.158.3.769-776.1984 PMID: 6373741